mTORC1 and mTORC2 have largely distinct functions in Purkinje cells

Angliker, Nico ; Burri, Michael ; Zaichuk, Mariana ; Fritschy, Jean-Marc ; Rüegg, Markus A

Abstract: The mammalian target of rapamycin (mTOR) is a key regulator of cellular growth which associates with other proteins to form two multi-protein complexes called mTORC1 and mTORC2. Dysregulation of mTORC1 signalling in brain is implicated in neuropathological conditions such as autism spectrum or neurodegenerative disorders. Accordingly, allosteric mTOR inhibitors are currently in clinical trials for the treatment of such disorders. Here, we ablated either mTORC1 or mTORC2 conditionally in Purkinje cells of the mouse cerebellum to dissect their role in the development, function and survival of these neurons. We find that the two mouse models largely differ from each other by phenotype and cellular responses. Inactivation of mTORC2, but not of mTORC1, led to motor coordination deficits at an early age. This phenotype correlated with developmental deficits in climbing fibre elimination and impaired dendritic self-avoidance in mTORC2-deficient Purkinje cells. In contrast, inactivation of mTORC1, but not of mTORC2, affected social interest of the mice and caused a progressive loss of Purkinje cells due to apoptosis. This cell loss was paralleled by age-dependent motor deficits. Comparison of mTORC1-deficient Purkinje cells with those deficient for the mTORC1 inhibitor TSC1 revealed a striking overlap in Purkinje cell degeneration and death, which included neurofilamentopathy and reactive gliosis. Altogether, our study reveals distinct roles of mTORC1 and mTORC2 in Purkinje cells for mouse behaviour and the survival of neurons. Our study also highlights a convergence between the phenotypes of Purkinje cells lacking mTORC1 activity and those expressing constitutively active mTORC1 due to TSC1 deficiency.

DOI: https://doi.org/10.1111/ejn.13051

Molecular & Synaptic Mechanisms

mTORC1 and mTORC2 have largely distinct functions in Purkinje cells

Nico Angliker[1], Michael Burri[1], Mariana Zaichuk[2], Jean-Marc Fritschy[2] and Markus A. Rüegg[1]

[1]Biozentrum, University of Basel, CH-4056 Basel, Switzerland

[2]Institute of Pharmacology and Toxicology, University of Zürich, CH-8057 Zurich, Switzerland

Running title: mTORC1 and mTORC2 inactivation in Purkinje cells

Keywords: mouse, cerebellum, raptor, rictor, TSC1

Number of pages: 46

Number of figures: 7

Number of tables and equations: 2 tables

Number of words in the (i) whole manuscript: 13769 (ii) Abstract: 248 (iii) Introduction: 421

Send correspondence to:

Markus A. Rüegg, PhD.
Biozentrum, University of Basel
Klingelbergstrasse 70
CH-4056 Basel, Switzerland
Phone: +41 61 267 22 23
Fax: +41 61 267 22 08
email: markus-a.ruegg@unibas.ch

ABSTRACT

The mammalian target of rapamycin (mTOR) is a key regulator of cellular growth that associates with other proteins to two multi-protein complexes, called mTORC1 and mTORC2. Dysregulation of mTORC1 signalling in brain is implicated in neuropathological conditions, such as autism spectrum or neurodegenerative disorders. Accordingly, allosteric mTOR inhibitors are currently in clinical trials for the treatment of such disorders. Here, we ablated either mTORC1 or mTORC2 conditionally in Purkinje cells of the mouse cerebellum to dissect their role in the development, function and survival of these neurons. We find that the two mouse models largely differ from each other by phenotype and cellular responses. Inactivation of mTORC2, but not of mTORC1, led to motor coordination deficits at an early age. This phenotype correlated with developmental deficits in climbing fibre elimination and impaired dendritic self-avoidance in mTORC2-deficient Purkinje cells. In contrast, inactivation of mTORC1, but not of mTORC2, affected social interest of the mice and caused a progressive loss of Purkinje cells due to apoptosis. This cell loss was paralleled by age-dependent motor deficits. Comparison of mTORC1-deficient Purkinje cells with those deficient for the mTORC1 inhibitor TSC1 revealed a striking overlap in Purkinje cell degeneration and death, which included neurofilamentopathy and reactive gliosis. Altogether, our study reveals distinct roles of mTORC1 and mTORC2 in Purkinje cells for mouse behaviour and the survival of neurons. Our study also highlights a convergence between the phenotypes of Purkinje cells lacking mTORC1 activity and those expressing constitutively active mTORC1 due to TSC1 deficiency.

INTRODUCTION

In mammalian cells, the serine/threonine protein kinase mTOR assembles into two multi-protein complexes, called mTORC1 and mTORC2. The two complexes share some proteins but differ for others. For example, raptor selectively associates with mTORC1 and is required for its function whereas rictor is only found in mTORC2 and is essential for its function (Laplante & Sabatini, 2012). mTORC1 controls cell growth and proliferation and integrates various signals from growth factors, energy status or amino acid availability and as output promotes protein synthesis, contributes to lipogenesis and inhibits autophagy (Shimobayashi & Hall, 2014). Growth factor signals converge on, and inhibit, the tuberous sclerosis complex (TSC), which is an upstream inhibitor of mTORC1. In contrast to mTORC1, activation of mTORC2 is less well understood, but it is well established that this complex phosphorylates and activates members of the AGC kinase family, including Akt, SGK1 and PKCs, which ascribes this complex a role in cell survival, metabolism and actin cytoskeletal organization (Oh & Jacinto, 2011). Ablation of raptor in the brain results in perinatal death of mice (Cloetta *et al.*, 2013). In contrast, whole-brain rictor knockout mice are viable but ataxic and they show a strong Purkinje cell phenotype (Thomanetz *et al.*, 2013). Recent reports have also shown that increased activation of mTORC1 in mouse Purkinje cells by conditional deletion of *Tsc1* or *Tsc2* or loss of one allele causes an autistic-like behaviour (Tsai *et al.*, 2012; Reith *et al.*, 2013). Concordantly, human patients suffering from the TSC disorder caused by mutations in the *TSC1* or *TSC2* gene are frequently autistic (Curatolo *et al.*, 2008). Thus, the cerebellum is not only important for motor control but is implicated in non-motor behaviour (Schmahmann *et al.*, 2007; Wang *et al.*, 2014). Importantly, the behavioural deficits of the conditional TSC1 knockout mice could be reversed by treatment with the mTORC1 inhibitor rapamycin (Tsai *et al.*, 2012). Consequently, rapamycin and analogues thereof (called rapalogs) are in clinical trials or are already on the market (everolimus) for the treatment of patients with TSC (Lipton & Sahin, 2014). However, little is known of how long-term

inactivation of mTORC1 affects mature neurons. Moreover, prolonged rapamycin treatment is known to also affect the function of mTORC2 (Sarbassov *et al.*, 2006). Hence, an analysis and comparison of mTORC1 and mTORC2 functions in developing and adult neurons is needed. Here, we addressed this question by conditionally deleting *Rptor* (gene encoding raptor) or *Rictor* in mouse Purkinje neurons. Our results show that the two complexes differentially affect synapse development, Purkinje cell survival and mouse behaviour.

MATERIALS AND METHODS

Mouse strains. All animal procedures complied with Swiss animal experimental regulations. C57BL/6 mice expressing the Cre recombinase under the endogenous *L7/Pcp-2* promoter *(L7/Pcp-2$^{Cre/+}$)* (Saito *et al.*, 2005) were crossed with mice carrying floxed alleles coding for raptor *(Rptor$^{loxp/loxp}$)*, rictor *(Rictor$^{loxp/loxp}$)* (Bentzinger *et al.*, 2008) or TSC1 *(Tsc1$^{loxp/loxp}$)* (Kwiatkowski *et al.*, 2002) to obtain the following mouse lines: *L7/Pcp-2$^{Cre/Cre}$; Rptor$^{loxp/loxp}$*, *L7/Pcp-2$^{Cre/Cre}$*; *Rictor$^{loxp/loxp}$* and *L7/Pcp-2$^{Cre/Cre}$*; *Tsc1$^{loxp/loxp}$* that were called RAPuKO, RIPuKO or TSCPuKO, respectively. Mice investigated were all homozygous for the *L7/Pcp-2-Cre* allele because of the higher percentage of recombination of the floxed alleles (Thomanetz *et al.*, 2013). Controls for RAPuKO, RIPuKO or TSCPuKO mice were proper littermates with the following genotype *L7/Pcp-2$^{Cre/Cre}$; Rptor$^{loxp/+}$*, *L7/Pcp-2$^{Cre/Cre}$; Rictor$^{loxp/+}$* and *L7/Pcp-2$^{Cre/Cre}$; Tsc1$^{loxp/+}$*, respectively. To label cells undergoing Cre-mediated recombination, a *Rosa26* locus-targeted EGFP reporter carrying a loxp stop cassette between the promoter and the coding sequence (*R26-EGFP$^{T/+}$* (Tchorz *et al.*, 2012)) was crossed into the RAPuKO or RIPuKO background. The resulting knockout mice of the following genotype *L7/Pcp-2$^{Cre/Cre}$; Rptor$^{loxp/loxp}$; R26-EGFP$^{T/+}$* and *L7/Pcp-2$^{Cre/Cre}$; Rictor$^{loxp/loxp}$; R26-EGFP$^{T/+}$* are referred to as RAPuKO GFP or RIPuKO GFP, respectively, and littermates of the *L7/Pcp-2$^{Cre/Cre}$; Rptor$^{loxp/+}$; R26-EGFP$^{T/+}$* and *L7/Pcp-2$^{Cre/Cre}$; Rictor$^{loxp/+}$; R26-EGFP$^{T/+}$* genotype were used as respective controls. For the conditional knockout of *Rptor* in neural progenitors (RAbKO), mice previously described were used (Cloetta *et al.*, 2013). Genotyping of the mice used toe tissue and was done as described elsewhere (Kwiatkowski *et al.*, 2002; Cloetta *et al.*, 2013; Thomanetz *et al.*, 2013). The *L7/Pcp-2$^{Cre/?}$* locus was detected using primers Fw 5' TGTGGCTGATGATCCGAATA and Bw 5' GCTTGCATGATCTCCGGTAT resulting in an amplicon of 249 bp. *L7/Pcp-2$^{Cre/Cre}$* mice were identified using primers Fw 5’ GAAGGCTTCTTCAACCTGCT and Bw 5’ ATATCCATGAGATTGTCCAT, resulting in the absence of a 292 bp. To detect EGFP

knocked-in at the *Rosa26* locus a nested PCR was performed using primers Fw 5' TGATATTGCTGAAGAGCTTGGCGGC and Bw 5' TGTGTGTATTCCTGGCTATCC for the first PCR (35 cycles) and Fw 5' AGCGCATCGCCTTCTATCGCC and Bw 5' TGATGTGTAGACCAGGCTGG for the second PCR (25 cycles) resulting in an amplicon of 253 bp.

Antibodies. β-Tubulin (Mouse, BD Pharmingen, #556321, 1:500), CAR8 (Goat, Watanabe lab (Patrizi *et al.*, 2008), 1:5000), calbindin D28k (Guinea pig, Synaptic Systems, #214 004, 1:500), calbindin D-28k (Mouse, Swant, #300, 1:2500), cleaved caspase-3 (Asp175) (Rabbit, Cell Signaling, #9661, 1:300), cytochrome c clone 6H2.B4 (Mouse, BD Pharmingen, #556432, 1:100), glial fibrillary acidic protein (GFAP) clone CA5 (Mouse, Millipore, #MAB360, 1:100), $GABA_A$ α1 subunit (Guinea pig, (Fritschy *et al.*, 2006), 1:5000), GAD65 (Monoclonal GAD-6, DSHB, Iowa, 1:1000), GFP (Chicken, Molecular probes, #A10262, 1:500), GSK3α (Rabbit, Cell Signaling, #9338, 1:1000), GSK3β (Rabbit, Cell Signaling, #9315, 1:1000), phospho-GSK3α/β (Ser21/9) (Rabbit, Cell Signaling, #9331, 1:1000), neurofilament H (Rabbit, Millipore, #AB1989, 1:200), phosphorylated neurofilaments (Mouse, Covance, #SMI-31P, 1:1000), phospho-S6 ribosomal protein (Ser235/236) (Rabbit, Cell Signaling, #2211, 1:100), PKCγ (Rabbit, Santa Cruz, #sc-211; 1:100), synaptophysin (Rabbit, GeneTex, #GTX100865, 1:100), fluorescein (DTAF) streptavidin (Jackson ImmunoResearch, #016-010-084, 1:300), Cy3-streptavidin (Jackson ImmunoResearch, #016-160-084, 1:1000)

Tissue homogenization and Western blot analysis. Brains were dissected, transferred to protein lysate buffer (50 mM Tris-HCl, pH 7.5, 150 mM NaCl, 1 mM EDTA, 1% Triton X-100 supplemented with EDTA-free protease inhibitor cocktail tablets (Roche), and phosphatase inhibitor tablets PhosSTOP (Roche)), and homogenized with a glass/Teflon homogenizer using 10 strokes at 800 rpm. The homogenate was centrifuged at 13,600 g for 15 min at 4°C. Cleared lysates were used to determine total protein amount (BCA Protein Assay;

Thermo Fisher Scientific). After dilution with 5x SDS sample buffer, equal protein amounts were loaded onto SDS gels.

Immunohistochemistry. Mice were deeply sedated with isoflurane. After decapitation, the brain was rapidly removed and immediately transferred into ice-cold, oxygenated (95% O_2, 5% CO_2), standard artificial cerebrospinal fluid (ACSF) containing (in mM) 119 NaCl, 1 NaH_2PO_4, 2.5 KCl, 2.5 $CaCl_2$, 1.3 $MgCl_2$, 11 D-glucose and 26.2 $NaHCO_3$. 250-µm-thick sagittal sections of cerebella were cut with a Leica VT1200S vibratome and transferred to oxygenated standard ACSF at room temperature and allowed to recover for about 30 min. Sections were fixed in 2-3 ml 4% paraformaldehyde (PFA) in PBS for at least 20 minutes and subsequently 3 times rinsed for 20 min with PBS. Slices were then stored overnight or longer at 4°C in 30% (w/v) sucrose in 0.1 M sodium phosphate buffer pH 7.4. The cryoprotected slices were then re-sliced as previously described (Schneider Gasser *et al.*, 2006). In brief, the slices were shortly rinsed in ice-cold PBS and then mounted on a pre-cut frozen block of O.C.T. (optimal cutting temperature compound) and stored for 30 min at -20°C. 15-µm-thick cryosections were made with a Leica CM1950 cryostat with a cryochamber and object head temperature of -20°C and -12°C, respectively, and subsequently stored at -20°C. Cryosections were thawed for about 2 min at 37°C and then incubated with blocking buffer (10% fetal bovine serum (FBS) and 0.2% Triton X-100 in PBS) for 1 h at room temperature. The primary antibodies were applied in blocking buffer overnight at 4°C and after washing in PBS (3 x 10 min), the corresponding secondary antibodies were added for 1 h at room temperature in blocking buffer. After washing in PBS (3 x 10 min), the slides were drained and coverslipped using Kaiser's glycerol gelatine (Merck, #1.09242.0100).

For $GABA_A$ α1 stainings, mice were deeply anesthetized with pentobarbital (Nembutal, 50 mg/kg, i.p.) followed by transcardiac perfusion with ice-cold standard ACSF at a flow rate of 10–15 ml/min (Notter *et al.*, 2014). The brains were extracted immediately after the perfusion and postfixed in ice-cold 4% PFA in 0.15 M sodium phosphate buffer, pH 7.4 for

90 min. Tissue was then cryoprotected with 30% sucrose in PBS (w/v). Sagittal sections (thickness 40 µm) were cut from frozen blocks with a sliding microtome (Microm Heidelberg, HM 400). Sections were collected in PBS and stored at -20°C in anti-freeze solution (15% glucose and 30% ethylene glycol in 50 mM sodium phosphate buffer, pH 7.4) prior use. Free-floating sections were incubated overnight at 4°C with primary antibodies and for 30 min at room temperature with secondary antibodies in Tris-HCl buffer, pH 7.4, containing 2% normal goat (or donkey) serum and 0.2% Triton X-100.

Fluoro-Jade B staining. Cryosections were thawed and dried at room temperature. The sections were first incubated for 5 min with 1% sodium hydroxide in 80% ethanol and then for 2 min with 70% ethanol for rehydration. The slides were transferred to 0.06% potassium permanganate for 10 min. Subsequently, they were rinsed for 2 min with ddH_2O and incubated with the staining solution for 20 min in the dark. The staining solution contained 2 µg/ml Fluoro-Jade B (FJB; Merck Millipore, #AG310) and 2 µg/ml Hoechst 33342 in 0.1% acetic acid. The slides were then washed three times 1 min in ddH_2O, drained and dried at 50°C. The dried slides were cleared in xylene for at least 1 min, drained and coverslipped using D.P.X. mounting medium (Sigma, #3176116).

Staining of biocytin-labelled Purkinje cells in acute slices. Purkinje cells were labelled with biocytin by the cell patch clamp method using intracellular solutions containing 3 mg/ml biocytin. The orientation of the acute slice was noted for the whole-cell recordings. The staining procedure was adapted from (Wierenga *et al.*, 2008). In brief, after the recording, slices were fixed overnight at 4°C in 4% PFA dissolved in PBS. Slices were extensively rinsed with PBS and subsequently incubated for 24 h at 4°C in blocking solution (10% FBS in PBS, containing 0.4% Triton X-100) on a shaker. The primary antibody was applied overnight at 4°C in blocking solution (5% FBS in PBS; 0.4% Triton X-100) on a shaker. After extensive washing with PBS, appropriate secondary antibodies were applied overnight at 4°C

in blocking solution. Acute slices were mounted in Kaiser's glycerol gelatine with the patched side facing up. Stained slices were analysed by confocal microscopy.

Image acquisition. Fluorescence pictures were taken using a Leica 5000B microscope with a 10x (NA 0.4) or 20x (NA 0.5) objective in combination with the software AnalySIS (Soft Imaging System). Confocal pictures were taken using the Leica TCS SPE confocal system with a 20x (NA 0.7), 40x (NA 1.15), 63x (NA 1.3) or 100x (NA 1.47) oil immersion objective or with a Zeiss LSM 710 microscope with a 63x lens (NA 1.4). For GFAP stainings whole automated multiple image acquisitions were made with the Olympus IX81 using a 10x objective (NA 0.3).

Quantification. For image analysis and processing, ImageJ was used. All analyses were done on sagittal sections of the cerebellar vermis. To analyse Purkinje cell density and soma size, fluorescence pictures of calbindin stainings taken from the cerebellar lobes IV & V using a 10x objective were used. Purkinje cell density was determined by dividing the number of Purkinje cells by the length of the analysed Purkinje cell layer segment and is indicated in cells per mm. Data of RIPuKO, RIPuKO GFP and corresponding control mice were pooled. For Purkinje cell soma size analysis, only somata were included where the primary dendrite was clearly visible. For each mouse, the mean Purkinje cell density and soma size of $n \geq 3$ cerebellar slices was determined.

Quantification of apoptotic cells, axonal swellings or FJB patches was done by counting their appearance in the entire cerebellar slice ($n \geq 3$ slices per mouse). For each mouse, the cerebellar slices were binned according to the number of observed events on the entire slice and finally the fraction of slices assigned to each bin was calculated. Apoptotic cells were positive for cleaved caspase-3 and showed a pyknotic nucleus. Calbindin staining was used to quantify axonal swellings of Purkinje cells in the granule cell layer.

The area covered by the dendritic tree of Purkinje cells was determined by merging *z*-stacks of confocal images (taken with 20x or 40x objectives) from biocytin-labelled Purkinje

cells that were detected by fluorescein (DTAF) streptavidin in acute slices. The entire dendritic tree was encircled by connecting the most apical points of the dendritic branches and the covered area was determined. Purkinje cell dendrite self-crossings were quantified on confocal pictures taken with a 63x objective from re-sliced (15 µm thick), biocytin-labelled Purkinje cells of RIPuKO GFP or corresponding control mice that were stained with Cy3-streptavidin. Merged *z*-stacks of confocal pictures taken from randomly chosen regions of spiny distal branches of biocytin-labelled cells were analysed for self-crossings. The number of dendritic self-crossings was normalized to the analysed area and the normalized values of RIPuKO GFP mice were then set in relation to the ones of control mice. The experimenter was blinded to the mouse genotype. $GABA_A$ α1 subunit clusters and GAD65-positive terminals were quantified based on threshold segmentation using self-written macros for ImageJ and Excel.

Electrophysiology. Sagittal cerebellar slices were prepared as described above in low calcium ACSF containing (in mM) 119 NaCl, 1 NaH_2PO_4, 2.5 KCl, 0.125 $CaCl_2$, 3.3 $MgCl_2$, 11 D-glucose and 26.2 $NaHCO_3$. Slices were then transferred for 30 min to 34°C-warm, oxygenated standard ACSF and subsequently stored in oxygenated standard ACSF at room temperature until they were used. Whole-cell recordings were taken at room temperature using an Axon MultiClamp 700A or 700B amplifier (Molecular Devices) and borosilicate glass pipettes (2-4 MΩ).

Internal solutions always contained biocytin (3 mg/ml) and cells were always analysed by immunohistochemistry as described above to confirm recombination of the targeted alleles in the recorded cell. The following internal solutions were used for the different recordings: for passive membrane properties (in mM) 140 K-gluconate, 4 NaCl, 2 $MgCl_2$, 5 HEPES, 1.1 EGTA, 2 Na_2-ATP, 0.6 mM Na_3-GTP, 5 sodium creatine phosphate, pH 7.3; for mEPSCs and mIPSC (in mM) 135 Cs-methanesulfonate, 8 NaCl, 10 HEPES, 0.5 EGTA, 4 Mg-ATP, 0.3 Na-GTP, 5 Lidocaine-N-ethyl bromide, pH 7.25; for climbing fibre stimulation (in mM) 150

CsCl, 1.5 mM $MgCl_2$, 10 HEPES, 0.1 EGTA, 2 Mg-ATP, 0.4 Na-GTP, 5 Lidocaine-N-ethyl bromide, pH 7.3; for LTD recordings (in mM) 65 Cs-methanesulfonate, 65 K-gluconate, 10 KCl, 1 $MgCl_2$, 20 HEPES, 0.4 EGTA, 4 Na_2-ATP, 1 mM Na_2-GTP, 5 sucrose, pH 7.3.

Passive membrane properties in RAPuKO, RAPuKO GFP, RIPuKO, RIPuKO GFP and corresponding control mice were measured in voltage clamp mode in response to a rectangular hyperpolarization from -60 mV to -80 mV for 300 ms using the pClamp system (Molecular Devices, version 10.2).

mEPSCs and mIPSCs were recorded in the presence of 0.5 µM TTX and at a holding potential of -70 mV and 0 mV, respectively, using the pClamp system. Traces were further analysed with the Mini Analysis Program v6 (Synaptosoft). Default settings of this program were used to automatically detect peaks. The peak detection algorithm is designed to first find a local maximum and then a baseline and subsequently differentiates between real peaks and noise-peaks by a threshold for the area under the curve. All detected events were manually cross-checked for correctness.

Climbing fibre innervation was analysed by placing a patch pipette (2 MΩ), filled with standard ACSF, in the granule cell layer in the vicinity of the patched Purkinje cell. Two current pulses (0.1 ms, paired-pulse interval: 62.5 or 100 ms) generated by a stable IS4 stimulator (SC-Devices) were applied every 20 s. The stimulation pipette was moved in the granule cell layer until the climbing fibre response (CF-EPSC) could be elicited with minimal stimulation intensity. The holding potential was set at -10 mV to inactivate voltage-gated conductances and to reduce the driving force. The stimulation intensity was reduced until all synaptic responses disappeared and was progressively increased again. The climbing fibre response as a function of the stimulation intensity was analysed and only events showing paired-pulse depression as well as a clear threshold were included for analysis. The number of innervating climbing fibres was estimated from the number of discrete CF-EPSC steps. Climbing fibre recordings were made and analysed using the pClamp system. For climbing

fibre analysis, 4-week-old RIPuKO and 12-week-old RIPuKO GFP mice and corresponding littermate control mice were used.

For LTD recordings, acute cerebellar slices were perfused with standard ACSF containing 100 μM picrotoxin (Sigma #P1675) and a patch pipette (2 MΩ) filled with perfusion solution was placed in the molecular layer in the vicinity of the voltage-clamped Purkinje cell. Parallel fibre (PF) responses were elicited by applying two current pulses using a stable IS4 stimulator (0.2 ms, paired-pulse interval: 100 ms) every 10 s while the cell was held at -60 mV. The stimulation intensity was chosen to obtain a PF-EPSC response of approximately -200 pA. A baseline was recorded for at least 10 min and when judged stable, LTD was induced by increasing the holding potential from -60 to +20 mV for 500 ms in conjunction with a single PF stimulus, which was repeated 30 times at a frequency of 1 Hz. Access resistance was measured every 10 s and recordings were discarded if it changed by more than 20% from the initial value. LTD was recorded and analysed using IGOR Pro software (WaveMetrics).

Behavioural assays. Mice were housed in a standard colony room with a 12:12 light:dark cycle and food and water was provided *ad libitum*. For behavioural tests, mice were transferred to a separate room at least 1 h prior to the experiment for adaptation. Tests were performed at the same time of day and the experimenter was blinded to the mouse genotype.

Balance beam test. For the balance beam test, a 70-cm-long, wooden beam, which was covered with masking tape, was horizontally connected to a dark box. The entire system was elevated to preventing mice to jump off. The starting area was brightly illuminated to motivate the mice to move towards the dark target box. The number of slips of the hind legs was counted. Mice were given 2 training sessions prior to the test session, each session consisted of 3 runs. During the training sessions, the diameter of the beam was gradually decreased. 4- to 8-week-old, female RIPuKO and 9- to 11-week-old, male RAPuKO mice and corresponding littermate controls were tested on a 1.1-cm-thick beam. For 14- to 20-week-

old, female RIPuKO and 29- to 41-week-old, male RAPuKO mice and the corresponding littermate controls, the diameter of the beam was 1.3 cm. For each mouse, the mean number of slips from three runs was calculated.

Footprint analysis. Paws of the mice were painted with non-toxic paint (forepaws in red, hindpaws in black). Mice were placed into an acrylic glass corridor of 1 m length and 8 cm width. The corridor was lined with white paper. The starting point was brightly illuminated to motivate the mouse to walk towards the dark box placed at the end of the corridor. For analysis, ten steps during which the mouse walked continuously and did not touch the wall were selected. The paper stripes were scanned, the coordinates of the footprints were evaluated using ImageJ and the mean gait width of the ten steps was calculated for each mouse. Female RIPuKO and male RAPuKO mice and corresponding littermate control mice of the indicated age were used for the footprint analysis.

Olfactory habituation/dishabituation. Olfactory habituation/dishabituation tests were performed as previously described (Yang & Crawley, 2009; Silverman *et al.*, 2010). 9- to 11-week-old male RAPuKO mice and 13- to 26-week-old RIPuKO and RIPuKO GFP mice and corresponding littermate control mice were used. In brief, mice were accommodated to a fresh cage with a clean and dry cotton tipped swab (cotton tip 2 cm over the cage ground) suspended from the cage lid for 30 min. After this acclimation period, odours were presented for 2 min in intervals of 1 min and the time of interest of the mouse in the cotton swab was measured. Interest was scored if the nose of the mouse was within 2 cm of the cotton tip. Odours were presented twice or three times to analyse olfactory habituation. The order of presented odours was water, water, banana, banana, social odour 1, social odour 1, social odour 1, social odour 2, social odour 2, social odour 2. For the water and banana odours, 100 µl of ddH_2O or isoamyl acetate (Sigma #W205532) diluted 1:1500 in ddH_2O were dripped onto the cotton tip. Social odours were obtained by wiping the cotton tipped swab in a zig-zag pattern across the bottom surface of a cage that had been used by 3-4 age-matched, unfamiliar

male mice of the same strain (C57BL/6) for 7 days. Results of RIPuKO and RIPuKO GFP mice and the corresponding control mice were pooled. Raw data were cleaned from statistical outliers by GraphPad prism software (ROUT method; Q = 0.1%) prior to statistical analysis.

Statistics. All data are presented as mean ± SEM. An unpaired Student's *t*-test or a one- or two-way ANOVA followed by a Tukey's or a Bonferroni's post hoc test was used to analyse data for statistical significance. A probability of 0.05 was taken as the level of statistical significance. Statistical analyses were performed using Prism software version 6.05 (GraphPad, San Diego, CA, USA).

RESULTS

Motor deficits and social behaviour of RAPuKO and RIPuKO mice

Purkinje cell-specific ablation of mTORC1 or mTORC2 was achieved by crossing *L7/Pcp-2-Cre* mice (Saito *et al.*, 2005) with *Rptor*$^{loxp/loxp}$ or *Rictor*$^{loxp/loxp}$ mice (Bentzinger *et al.*, 2008) as previously described (Thomanetz *et al.*, 2013). The resulting mouse lines are called RAPuKO or RIPuKO (for raptor- or rictor Purkinje cell knockout). *L7/Pcp-2*-driven Cre expression starts at embryonic day 17.5 (E17.5) (Saito *et al.*, 2005) and hence this Cre driver deletes the targeted alleles during Purkinje cell development (Watanabe & Kano, 2011).

As Purkinje cells provide the sole output of the cerebellar cortex and are known to be essential for motor control, we first analysed how raptor and rictor depletion affected motor coordination. For this reason, RAPuKO and RIPuKO mice were tested on a balance beam and the number of hind leg slips that occurred during the crossing was counted. In RIPuKO mice, the number of slips was significantly increased compared to control littermates independent of age (4-8 weeks: $t_{21} = 2.6$, $P = 0.017$; 14-20 weeks: $t_{17} = 3.2$, $P = 0.0054$; Fig. 1A). In contrast, young RAPuKO mice did not show any motor coordination deficits, whereas a significant deficit was noted at the age of 29-41 weeks (9-11weeks: $t_{23} = 0.94$, $P = 0.36$; 29-41 weeks: $t_{32} = 3.07$, $P = 0.0044$; Fig. 1B). In addition to the early-onset coordination deficits, RIPuKO mice showed an increase in the gait width of their hind legs ($t_{16} = 2.99$, $P = 0.0087$; Fig. 1C), whereas RAPuKO mice did not show any change in gait ($t_{15} = 0.53$, $P = 0.61$; Fig. 1D;). Thus, mTORC2 deficiency in Purkinje cells results in early deficits in motor coordination whereas inactivation of mTORC1 affects this behaviour only at a rather high age.

Recent reports have shown that Purkinje cell-specific depletion of TSC1, which results in sustained activation of mTORC1, causes autism spectrum disorder-like changes in mice that manifest by altered social behaviour (Tsai *et al.*, 2012). To evaluate whether a similar phenotype could also be noted in mice deficient for mTORC1, we tested RAPuKO mice in an

olfactory habituation/dishabituation test. To rule out that motor deficits interfered with this test, we used young mice. While RAPuKO mice spent the same time sniffing non-social odours as control mice, the interest in social odours was significantly reduced ($F_{1,218} = 24.3$, $P < 0.01$; Fig. 1F). As depletion of TSC1 also affects mTORC2 signalling (Goto *et al.*, 2011; Carson *et al.*, 2012), we also tested RIPuKO mice in the same behavioural paradigm. However, no significant difference in the interest in either non-social or social odours was observed ($F_{1,381} = 7.5$, $P > 0.05$; Fig. 1E). These data indicate that mTORC1 and mTORC2 have distinct functions in Purkinje cells as the phenotypes in motor coordination and social interest are distinct.

Morphology and synaptic alterations in Purkinje cells of RAPuKO mice

Expression of Cre under the control of the *L7/Pcp-2* promoter is mosaic in Purkinje cells (Saito *et al.*, 2005). Similarly, we have previously shown that rictor is depleted in only 75% of the Purkinje cells in RIPuKO mice and that lack of expression of PKCγ is a reliable marker for successful removal of rictor (Thomanetz *et al.*, 2013). To test whether a similar mosaic pattern was observed in RAPuKO mice, we stained sagittal sections of the cerebellum for the phosphorylated form of S6 (pS6), which is activated by mTORC1 (Wullschleger *et al.*, 2006). Thus, lack of pS6 was used as an indicator of successful depletion of raptor. In young, 3- to 11-week-old RAPuKO mice, 49 ± 5% (mean ± SEM; n = 19 mice) of the Purkinje cells were negative for pS6 (pS6(-)) while all Purkinje cells of control mice were pS6-positive (pS6(+)) (Fig. 2A). To validate that lack of pS6 was indeed indicative of raptor depletion, a GFP reporter mouse for Cre-mediated recombination (Tchorz *et al.*, 2012) was crossed into the RAPuKO background. In those mice, called RAPuKO GFP, 98 ± 1% (mean ± SEM; n = 3 mice) of the pS6(-) Purkinje cells of 11-week-old mice were also GFP-positive (GFP(+)) whereas 83 ± 3% (mean ± SEM; n = 3 mice) of the pS6(+) Purkinje cells were GFP-negative ((GFP(-)). In comparison to GFP(-)/pS6(+) Purkinje cells, the soma size of GFP(+)/pS6(-)

Purkinje cells was reduced by 59% ($F_{2,6}$ = 129.4, P < 0.0001; Supporting fig. 1A and C), consistent with the role of mTORC1 in the control of cell size. 10% of Purkinje cells of RAPuKO GFP mice were GFP(+) and pS6(+) (Supporting fig. 1A and B). Together, these data show that lack of pS6 is a reliable marker for raptor depletion in Purkinje cells.

A reduction in soma size by 40-50% could be detected in the pS6(-) Purkinje cells of RAPuKO mice already at the age of 3 weeks when compared to Purkinje cells of age-matched control mice ($F_{2,6}$ = 28.3, P = 0.0017; Fig. 2B). Notably, this reduction remained the same in RAPuKO mice at higher age (6 weeks: $F_{2,8}$ = 32.8, P = 0.0009; 11 weeks: $F_{2,9}$ = 28.3, P = 0.0026; 20-42 weeks: $F_{2,9}$ = 59.1, P = 0.001; Fig. 2B). On the other hand, a small but significant increase in the soma size of the pS6(+) Purkinje cells in older RAPuKO mice could be observed in comparison to Purkinje cells of the corresponding control mice (20-42 weeks: $F_{2,9}$ = 59.1, P = 0.0011; Fig. 2B). Next to a reduction in soma size, raptor-depleted Purkinje cells also showed a decrease in the area covered by the dendritic tree by 42 ± 3% (mean ± SEM; n ≥ 36 cells using n = 7 mice; two-tailed Student's t-test: t_{74} = 9.1, P < 0.0001; Fig. 2C). Additionally, more than 40% of raptor-depleted Purkinje cells of 4- to 6-week-old RAPuKO mice contained multiple primary dendrites (Fig. 2C and D) while ~90% of Purkinje cells in control mice had only one primary dendrite. Multiple primary dendrites at a similar frequency were also observed in RIPuKO mice (Thomanetz *et al.*, 2013). However, Purkinje cells of RAPuKO mice were all positive for the mTORC2 downstream target PKCγ (Fig. 2E), indicating that mTORC1 ablation in Purkinje cells does not affect mTORC2 signalling, in line with previous data (Cloetta *et al.*, 2013). In summary, raptor depletion in Purkinje cells results in severe, morphological changes. Although rictor depletion also affects the size of Purkinje cells (Thomanetz *et al.*, 2013), the effect in RAPuKO mice is much stronger.

To test whether the morphological changes in raptor- and rictor-deficient Purkinje cells resulted in changes in their function, passive membrane properties were next measured in whole-cell recordings. Purkinje cells in RAPuKO mice were selected by their soma size,

patched and recorded with pipettes filled with biocytin. After recording, the morphology of the recorded, biocytin-filled Purkinje cell was visualized and raptor deficiency was confirmed by pS6 staining (Supporting fig. 2A - C). As expected from the small soma size of raptor-depleted Purkinje cells, capacitance was decreased ($F_{2,55}$ = 289.8, P < 0.0001; Supporting fig. 2D) and membrane resistance was increased ($F_{2,55}$ = 56.9, P < 0.0001; Supporting fig. 2E). Both parameters were also altered in RIPuKO mice (capacitance: t_{44} = 6.3, P < 0.0001; membrane resistance: t_{44} = 5.3, P < 0.0001; Supporting fig. 2D and E), consistent with the previous finding that their somata are smaller (Thomanetz *et al.*, 2013). Hence, the reduction of the soma size and the concomitant alterations of their passive membrane properties are reliable markers for raptor deficiency.

Synapse function was examined by measuring miniature excitatory and inhibitory postsynaptic currents (mEPSC and mIPSC, respectively). While there was no difference in the mEPSCs of raptor-deficient Purkinje cells at the age of 6 weeks compared to cells in control mice (mEPSC frequency: t_{24} = 0.49, P = 0.63; mEPSC amplitude: t_{24} = 0.056, P = 0.96; Fig. 3A – C), a pronounced reduction in the frequency of mIPSCs (t_{28} = 4.065, P = 0.0004; Fig. 3D and E), but not the amplitude (t_{28} = 0.22, P = 0.83; Fig. 3D and F), was observed. By quantitative immunohistochemistry using antibodies against the α1 subunit of $GABA_A$ receptors, we also found that the mean number of $GABA_A$ α1 clusters on the somata of pS6(-) Purkinje cells was reduced by 43% (t_8 = 4.46, P = 0.0021; Fig. 3G and I). In contrast, no change in the density of the $GABA_A$ α1 clusters was seen in the molecular layer (t_7 = 0.15, P = 0.88; Fig. 3H and J), which might be based on the high percentage (~40%) of inhibitory synapses on interneurons (Briatore *et al.*, 2010). Interneurons are not targeted by the conditional knockout. Together, our data indicate a lowering of the number of inhibitory synapses formed onto raptor-deficient Purkinje cells.

Raptor deficiency also affected the size of GABAergic synapses but this effect differed between the soma and the molecular layer. While the size of $GABA_A$ α1 clusters on the

somata of raptor-deficient Purkinje cells was increased (t_{1644} = 5.9, P < 0.0001; Fig. 3K), the size of GAD65/$GABA_A$ α1-positive clusters in the molecular layer was smaller (t_{1384} = 2.81, P = 0.005; Fig. 3L), which may explain why we could not detect any alteration in the amplitude of the mIPSCs as the size differences may cancel each other out. In summary, these data indicate a misbalance between the inhibitory and the excitatory input in Purkinje neurons that are deficient of raptor. Such a misbalance, in turn, might contribute to the behavioural deficit in social interest of RAPuKO mice. Noteworthy, rictor knockout in Purkinje cells affects both excitatory and inhibitory synaptic properties (Thomanetz *et al.*, 2013).

Multiple climbing fibre innervation accounts for ataxia of RIPuKO mice

Rictor knockout in Purkinje cells is paralleled by a striking down regulation of PKCγ (Thomanetz *et al.*, 2013), the major PKC isoform expressed by these neurons (Barmack *et al.*, 2000). Mice with a conventional knockout of PKCγ show impaired motor coordination (Chen *et al.*, 1995). This motor coordination deficit is paralleled by multiple innervation of Purkinje cells by climbing fibres (CF) (Kano *et al.*, 1995). As RIPuKO mice showed a motor coordination phenotype (Fig. 1), we analysed CF innervation by measuring EPSCs in Purkinje cells by whole-cell recordings in response to electrical stimulation of CFs. Several parameters of the CF-EPSCs were altered in rictor-deficient Purkinje cells (Table 1), which is probably due to their morphological changes. When we analysed mice at the age of 4 weeks, which is one week after synapse elimination is completed (Hashimoto & Kano, 2013), more than 90% of the control Purkinje cells showed uniform CF-EPSCs, indicative of single CF innervation (Fig. 4A and D). In contrast, several distinct CF-EPSCs were measured for ~ 40% of Purkinje cells in RIPuKO mice, indicative of multiple innervation (Fig. 4B and D). In addition, paired-pulse depression (PPD) of CF synapses was slightly increased in RIPuKO compared to control mice (Fig. 4B; Table 1). To rule out that multiple CF innervation was simply due to a delay in CF elimination, we also measured CF-EPSC responses in 12-week-old RIPuKO

mice. The percentage of knockout cells showing multiple discrete steps in CF-EPSC responses was very similar to those in young mice (Fig. 4C and D), indicating that multiple CF innervation of rictor-knockout Purkinje cells persists throughout adulthood. Hence, multiple CF innervation, like in PKCγ knockout mice, might be responsible for the motor deficits in RIPuKO mice. In contrast, 4-week-old RAPuKO mice did not show multiple CF innervation (Fig. 4E – G). However, similar to rictor-deficient Purkinje cells, PPD of CF-EPSCs was slightly increased in raptor-depleted Purkinje cells and morphological changes were also paralleled by altered CF-EPSC properties (Table 1).

Another cellular correlate implicated in altered motor behaviour is a failure to undergo cerebellar long-term depression (LTD) (Kano *et al.*, 2008; Hirano, 2013). Cerebellar LTD is induced by simultaneous stimulation of parallel fibre (PF) and CF synapses, which leads to a profound depolarization of the Purkinje cell and a weakening of the PF synapse. Because rictor-deficient Purkinje cells are frequently innervated by multiple CFs, LTD was induced by directly depolarizing the voltage-clamped Purkinje cell via the recording electrode and simultaneously stimulating the PFs (Fig. 4H) (Kakegawa *et al.*, 2011). Although some of the kinetics of the PF-EPSCs was slightly altered in RIPuKO mice (Table 1), the LTD-inducing protocol caused a similar reduction of the PF-EPSCs in both control and rictor-deficient Purkinje cells ($t_{15} = 0.33$, $P = 0.74$ (analysed 30 min after LTD induction); Fig. 4I - K). These experiments show that cerebellar LTD is normal in RIPuKO mice and thus exclude this as a mechanism responsible for the changed motor behaviour.

Impairment of gait and motor coordination has also been correlated with an increased number of dendritic self-crossings of Purkinje cells, which has been suggested to result from defective dendritic self-avoidance (Gibson *et al.*, 2014). Impaired dendritic self-avoidance is evident in Purkinje cells deficient of γ-protocadherins (Lefebvre *et al.*, 2012), a class of molecules that acts via the mTORC2 target PKC (Garrett *et al.*, 2012). Thus, we analysed dendritic self-avoidance in 12-week-old RIPuKO mice by re-slicing biocytin-labelled

Purkinje cells and staining them for Cy3-streptavidin and PKCγ. Confocal microscopy analysis of randomly selected regions of spiny distal branches of the dendritic tree (Fig. 4L and M) revealed a significant increase in the number of dendritic self-crossings in rictor-knockout Purkinje cells ($t_{67} = 4.7$, $P < 0.0001$; Fig. 4N). Hence, loss of mTORC2 in Purkinje cells also decreases dendritic self-avoidance. In summary, failure in CF synapse elimination and hampered self-avoidance of dendrites might both contribute to the motor coordination phenotype of RIPuKO mice. Interestingly, both of those cellular phenomena have previously been linked to dysregulation of the mTORC2 target PKC.

Age-dependent loss of Purkinje cells in RAPuKO but not RIPuKO mice due to apoptosis

As described above, the motor coordination phenotype of RIPuKO mice was observed at an early age whereas the motor coordination deficits of RAPuKO mice were only observed at higher age. This together with the previous finding that ablation of mTORC1 causes increased apoptosis of neurons (Cloetta *et al.*, 2013), led us to hypothesize that loss of Purkinje cells might underlie the age-dependent motor deficits of RAPuKO mice. To test this, we counted the number of Purkinje cells in RAPuKO and RIPuKO mice in the course of mouse ageing. While the density of the Purkinje cells remained the same in RIPuKO mice (3 weeks: $t_4 = 0.044$, $P = 0.97$; 18 weeks: $t_4 = 0.62$, $P = 0.57$; 86-96 weeks: $t_4 = 1.77$, $P = 0.15$; Fig. 5A and B), it significantly decreased in RAPuKO mice older than 11 weeks (3 weeks: $t_5 = 1.46$, $P = 0.21$; 6 weeks: $t_9 = 0.62$, $P = 0.55$; 11 weeks: $t_6 = 2.31$, $P = 0.06$; 17-29 weeks: $t_4 = 6.2$, $P = 0.0034$; 41-42 weeks: $t_4 = 7.75$, $P = 0.0015$; Fig. 5C and D). To investigate whether cell loss was due to apoptosis, cells were stained for cleaved caspase-3 (CC3), a well-known apoptosis marker (Gown & Willingham, 2002). No CC3-positive Purkinje cells ($CC3^+$ PCs) were found in 6-week-old RAPuKO mice (data not shown) but many positive cells could be detected at the age of 11 weeks ($t_6 = 5.26$, $P = 0.0019$ (bin: 1 $CC3^+$ PC per slice); Fig. 5E and F). Those cells also showed signs of a condensed and fragmented nucleus in the Hoechst staining (Fig.

5E), which is an additional characteristic of apoptosis (Robertson *et al.*, 2000). The apoptotic events were also accompanied by the appearance of GFAP-positive fibres in the molecular layer (Fig. 5G and H). The localization of the GFAP-positive fibres and their palisade-like arrangement (Fig. 5H) suggested that these were Bergmann glia cells, which are known to be closely associated with Purkinje cells (Yamada & Watanabe, 2002). An increase of GFAP-positive fibres is a hallmark of reactive astrogliosis that can be a consequence of neurodegeneration (Pekny & Nilsson, 2005). Thus, at a higher age, Purkinje cells in RAPuKO mice are lost because of apoptosis. Most probably, the age-dependent loss of Purkinje cells underlies the motor coordination deficits that are visible in old RAPuKO mice.

Neurofilamentopathy upon ablation or sustained activation of mTORC1 in Purkinje cells

To further investigate the cause of cell death in RAPuKO mice, we next stained for degenerating neurons using Fluoro-Jade B (FJB), a compound that specifically stains degenerating neurons (Schmued & Hopkins, 2000). FJB-positive puncta were visible in the molecular and Purkinje cell layer of 6- and 11-week-old RAPuKO but not of control mice (6 weeks: $t_4 = 8.0$, $P = 0.0013$ (bin: 1-5 FJB patches); 11 weeks: $t_4 = 4.0$, $P = 0.016$ (bin: 6-10 FJB patches); Fig. 6A and B), indicating that neurodegeneration preceded apoptosis in raptor-knockout Purkinje cells. In addition, signs of dendritic atrophy and beading could be detected in biocytin-labelled, raptor-deficient Purkinje cells of 6-week-old mice (Fig. 6C) and swellings of axons proximal to raptor-deficient Purkinje cell somata were often detected whereas such swellings were only very rarely observed in control mice (6 weeks: $t_6 = 3.27$, $P = 0.017$ (bin: 1-5 swellings); 11 weeks: $t_6 = 15.0$, $P < 0.0001$ (bin: 5< swellings); Fig. 6D - H). Swollen axons are thought to be an early sign of axonal degeneration and have been reported to frequently contain organelles or cargo proteins, such as mitochondria, synaptic vesicles and neurofilaments (Ching *et al.*, 1999; Louis *et al.*, 2009; Watanabe *et al.*, 2010;

Yang *et al.*, 2013). In accordance, 84.8 ± 0.7% (mean ± SEM; n = 390 swellings of n = 4 mice) of the axonal swellings in RAPuKO mice were strongly positive for neurofilament heavy (neurofilament H) (Fig. 6D) and 81.2 ± 5% (mean ± SEM; n = 196 swellings of n = 4 mice) were positive for the phospho-neurofilament epitope (SMI31) (Fig. 6E). In contrast, the swellings did not show any accumulation of mitochondria (Fig. 6F) or synaptic vesicles (Fig. 6G). Neurofilaments are known to undergo axonal transport and there is evidence that this is regulated by phosphorylation in the C-terminal KSP repeats (reviewed in (Shea *et al.*, 2009; Holmgren *et al.*, 2012)), and glycogen synthase kinase 3 (GSK3) has been shown to phosphorylate neurofilament H at the KSP repeats (Bajaj & Miller, 1997). Because phosphorylation of GSK3α/β at residue Ser21/9 is downstream of Akt (Cross *et al.*, 1995) and because changes in mTORC1 activity affect activation of Akt (Bentzinger *et al.*, 2008), we examined phosphorylation of GSK3 in mice that lack raptor in all brain cells (Cloetta *et al.*, 2013). In those mice, phosphorylation of GSK3 was strongly increased (P-GSK3α: $t_8 = 5.3$, $P = 0.0007$; P-GSK3β: $t_8 = 6.29$, $P = 0.0002$; GSK3α: $t_8 = 1.55$, $P = 0.16$; GSK3β: $t_8 = 0.88$, $P = 0.41$; Fig. 6I and J), indicating that aberrant GSK3 signalling might be the cause of the axonal accumulation of neurofilaments in raptor-knockout Purkinje cells.

Similar proximal axonal swellings have also been reported in mice deficient for TSC1 in Purkinje cells (Tsai *et al.*, 2012). Because TSC1 knockout in brain tissue is known to affect GSK3 signalling (Meikle *et al.*, 2008), we hypothesized that the swollen axons in TSC1-deficient Purkinje cells might also contain neurofilaments. Indeed, axonal swellings in 11-week-old TSC1 Purkinje cell knockout (TSCPuKO) mice were in 78.5 ± 3% (mean ± SEM; n = 266 swellings of n = 4 mice) and 79.6 ± 2% (mean ± SEM; n = 276 swellings of n = 4 mice) of the cases clearly positive for neurofilament H (Fig. 7A) and phosphorylated neurofilament (Fig. 7B), respectively. At this age, few Purkinje cells underwent apoptosis and their density was reduced (data not shown), consistent with the observations by others (Tsai *et al.*, 2012) that TSC1 deficiency reduces Purkinje cell survival. Like in RAPuKO mice, Purkinje cell

degeneration/apoptosis in TSCPuKO mice was paralleled by reactive Bergmann glia that manifested in palisade-like, GFAP-positive structures in the molecular layer (Fig. 7C). Altogether, these data show that both, ablation and sustained activation of mTORC1, results in a neurofilamentopathy, accompanied by the accumulation of neurofilaments in the axonal swellings proximal to the somata of Purkinje cells, and causes Purkinje cell death by apoptosis.

DISCUSSION

Here, we describe the phenotypes of mice that lack mTORC1 or mTORC2 in developing and adult Purkinje cells. While some of the phenotypes, such as the changes in cell morphology, are shared between RAPuKO and RIPuKO mice, most of them differ between the two mouse models (Table 2). Phenotypes that are exclusive for the RAPuKO mice are (*i*) the reduced social interest and (*ii*) the progressive loss of Purkinje cells that starts at the age of 11 weeks (Table 2). Phenotypes exclusive to RIPuKO mice are (*i*) the early changes in motor coordination and the gait alterations and (*ii*) the impairment of CF synapse elimination (Table 2). Thus, our work provides strong evidence that mTORC1 and mTORC2 have only a few common but many very distinct functions in Purkinje neurons although they share many of the molecular components including mTOR.

A role of mTORC1 for the morphology of Purkinje cells

Given the important role of mTORC1 for cell growth (Wullschleger *et al.*, 2006), our observation that raptor-deficient Purkinje cells have smaller cell somata and a smaller dendritic tree is not surprising. The size difference was seen already at 3 weeks of age and persisted throughout adulthood. Thus, raptor-deficient Purkinje cells seem to never reach the size of wild-type neurons. The observed change of the dendritic tree in raptor-deficient Purkinje cells and, in particular, the presence of several primary dendrites was, however, not expected. The development of the Purkinje cell dendrites occurs mainly in the first three postnatal weeks. Purkinje cells transiently express multiple primary dendrites around birth and all but one are subsequently eliminated within the first two weeks. Later, the final size of the dendritic tree is established by a rapid and a slow growth phase (Sotelo & Dusart, 2009). While the detailed molecular mechanisms involved in this developmental reshaping of the dendrites are not well established, neuronal polarity is regulated by the PI3K-Akt-GSK3 pathway (Arimura & Kaibuchi, 2007) and inhibition of GSK3 by phosphorylation increases

the number of primary dendrites in cultured neurons (Naska *et al.*, 2006). Finally, brain-specific deletion of the PI3K-Akt inhibitor PTEN results in the formation of ectopic dendrites in neurons, which correlates with increased phosphorylation of Akt and GSK3 (Kwon *et al.*, 2006). Inactivation of mTORC1 by raptor depletion increases Akt signalling (Cloetta *et al.*, 2013) because the inhibitory feedback loop via S6K is dampened (Um *et al.*, 2004). Thus, increased GSK3 inhibition because of Akt-mediated phosphorylation in raptor-deficient Purkinje neurons may cause the multiple primary dendrites.

Interestingly, Purkinje cells deficient for rictor have also several primary dendrites (Thomanetz *et al.*, 2013). Despite the similar phenotype to the RAPuKO mice, the underlying mechanism in RIPuKO mice is more likely based on abnormal PKC signalling including the dysregulation of its downstream targets MARCKS and GAP-43, as previously commented (Angliker & Ruegg, 2013). Consistent with this PKC-mediated mechanism, rictor-deficient Purkinje cells also exhibit extensive self-crossings of spiny distal dendritic branches. A very similar phenotype was also observed in mice deficient for γ-protocadherins, which also affect PKC signalling and its downstream target MARCKS (Garrett *et al.*, 2012; Lefebvre *et al.*, 2012).

Effect of mTORC1 and mTORC2 on synaptic connectivity

While there is morphological similarity between Purkinje cells in RAPuKO and RIPuKO mice, alterations in their synaptic connectivity are rather distinct (Table 2). For example, excitatory synapses are not altered in raptor-depleted Purkinje cells as judged by their mEPSC amplitude or frequency, whereas rictor-depletion results in a strong reduction of mEPSC frequency (Thomanetz *et al.*, 2013). Consistent with a function of mTORC2 at excitatory synapses, others have shown that late-phase LTP is affected in rictor-depleted hippocampal neurons due to impaired actin polymerization (Huang *et al.*, 2013). We here also show that elimination of excitatory CF synapses is hampered in RIPuKO mice while LTD at PF-

Purkinje cell synapses is not affected. The same phenotype has been reported in PKCγ knockout mice (Chen *et al.*, 1995). Mechanistically, this phenotype has been explained by the role of PKC in postsynaptic mGluR1 signalling (Chen *et al.*, 1995; Kano *et al.*, 1995; Offermanns *et al.*, 1997; Kano *et al.*, 1998; Ichise *et al.*, 2000), which drives CF synapse elimination via its regulating PF synaptic input (Kakizawa *et al.*, 2000; Hashimoto & Kano, 2013). Concordantly, Purkinje cells in mice deficient for PKCγ or other downstream regulators of mGluR1 signalling are innervated by multiple CFs and the mice show motor deficits.

Similar to excitatory, also inhibitory synaptic input is differently affected in RAPuKO and RIPuKO mice: RAPuKO mice show a pronounced reduction of mIPSC frequency whereas only small changes in mIPSC amplitude have been observed in RIPuKO mice (Table 2) (Thomanetz *et al.*, 2013). Consistent with the reduced mIPSC frequency of raptor-deficient Purkinje cells, the number of perisomatic $GABA_A$ α1 clusters was reduced. Raptor knockout also affected the size of $GABA_A$ α1 clusters but the effect depended on the subcellular localization. While $GABA_A$ α1 cluster size was increased on the somata of Purkinje cells, it was decreased in the dendrites (i.e. the molecular layer). In rats, the size of $GABA_A$ α1 clusters on the soma of Purkinje cells has been shown to become reduced during the first three postnatal weeks whereas the size of $GABA_A$ α1 clusters in the molecular layer is increased (Viltono *et al.*, 2008). As $GABA_A$ α1 cluster size is increased on the soma of knockout cells but decreased in the molecular layer in 6-week-old RAPuKO mice, it is possible that these changes are a consequence of impaired postnatal development of GABAergic synapses.

There is also evidence that mTOR binds to gephyrin (Sabatini *et al.*, 1999), an important postsynaptic scaffolding protein at inhibitory synapses (Tyagarajan & Fritschy, 2014). A more recent study has shown that phosphorylation of gephyrin residue Ser200 is rapamycin-sensitive (Demirkan *et al.*, 2011). Moreover, rapamycin treatment of cultured hippocampal

neurons causes a reduction in the density of gephyrin clusters (Wuchter *et al.*, 2012). Therefore, it is possible that impaired gephyrin clustering underlies the altered inhibitory synaptic input of raptor-depleted Purkinje cells. Furthermore, the mTORC2 downstream targets PKC and Akt phosphorylate the β2 subunit of $GABA_AR$ (McDonald & Moss, 1997; Wang *et al.*, 2003) and Akt increases surface expression of $GABA_AR$ (Wang *et al.*, 2003). Consequently, mTORC2 ablation may negatively affect the surface expression of $GABA_AR$ and hence lower inhibitory synaptic currents.

Convergent phenotypes of sustained activation or inactivation of mTORC1 in Purkinje cells

Another interesting aspect of our work is the rather similar phenotypes of RAPuKO and TSCPuKO mice although the immediate downstream signalling is the opposite. For example, both mouse models show a strong accumulation of neurofilaments in axonal swellings and a progressive loss of Purkinje cells due to apoptosis, which is paralleled by reactive gliosis. We also provide evidence that aberrant GSK3 signalling may underlie this convergence in the neurofilamentopathy as phosphorylation of GSK3 is strongly increased in lysates from raptor-deficient brains and GSK3 signalling is also altered in mice deficient for TSC1 in the brain (Meikle *et al.*, 2008). GSK3 phosphorylates neurofilaments at the E-segment (Sasaki *et al.*, 2002; Sasaki *et al.*, 2009) and KSP repeats (Bajaj & Miller, 1997). While phosphorylation of KSP repeats is crucial for various functions including axonal transport (Shea *et al.*, 2009; Holmgren *et al.*, 2012), the E-segment has been suggested to affect the conformation of the C-terminal KSP repeats (Sasaki *et al.*, 2009). Thus, differential modification of the neurofilaments in the RAPuKO and TSCPuKO mice by GSK3 may result in a similar functional effect.

Besides the similarity in the neurodegenerative phenotype, RAPuKO and TSCPuKO mice also share behavioural similarities. Like in TSCPuKO mice (Tsai *et al.*, 2012), the social

interest of RAPuKO mice was reduced at young age, when the Purkinje cell density was still unaffected. Alterations in inhibitory synaptic input and in dendritic morphology in the RAPuKO mice discussed above might underlie this abnormal social behaviour. A similar convergence of the phenotypes has been observed in mice deficient for raptor or TSC1 in skeletal muscle. In both cases the genetic manipulations result in myopathies that are characterized by vacuoles (Bentzinger *et al.*, 2008; Castets *et al.*, 2013). In skeletal muscle, changes in autophagy flux, although at different levels of the process, might underlie this convergence. In summary, our findings demonstrate that both, sustained activation and inhibition of mTORC1 in Purkinje cells, affect non-motor functions of the cerebellum and, at later time points, the survival of these neurons. Consequently, our data advice caution in treating brain disorders with rapamycin or other mTORC1 inhibitors, as has recently been suggested (Santini & Klann, 2011; Costa-Mattioli & Monteggia, 2013).

ACKNOWLEDGEMENTS

We thank Dr. J. S. Tchorz and Prof. B. Bettler for providing a *Rosa26* reporter line, Prof. P. Scheiffele for the *L7/Pcp-2 Cre* line and Dr. E. Pérez-Garci and Dr. J. R. Reinhard for comments on the manuscript. The monoclonal antibody GAD-6, developed by Dr. D.I. Gottlieb, was obtained from the Developmental Studies Hybridoma Bank, created by the NICHD of the NIH and maintained at the University of Iowa, Department of Biology, Iowa City, IA 52242. The Car8 antibody was obtained from Dr. Masahiko Watanabe, Hokkaido University Graduate School of Medicine, Sapporo, Japan. This work was supported by the Cantons of Basel-Stadt and Baselland (MAR) and a Sinergia grant of the Swiss National Science Foundation to MAR and JMF. The authors declare no competing financial interests.

ABBREVIATIONS

Akt/PKB, protein kinase B; Car8, carbonic anhydrase 8; CC3, cleaved caspase-3; CF, climbing fibre; EPSC, excitatory postsynaptic currents; FJB, Fluoro-Jade B; GABA, gamma-aminobutyric acid; $GABA_AR$, $GABA_A$ receptor; GAD65, glutamic acid decarboxylase 65 kDa; GAP-43, growth associated protein 43; GCL, granule cell layer; GFAP, glial fibrillary acidic protein; GFP, green fluorescent protein; GSK3α/β, glycogen synthase kinase 3α/β; IPSC, inhibitory postsynaptic currents; LTD, long-term depression; LTP, long-term potentiation; MARCKS, myristoylated alanine-rich C-kinase substrate; mEPSC/mIPSC, miniature excitatory/inhibitory postsynaptic currents; mGluR1, metabotropic glutamate receptor 1; ML, molecular layer; mTOR, mammalian target of rapamycin; mTORC1/mTORC2, mammalian TOR complex 1/2; PF, parallel fibre; PI3K, phosphatidylinositol-3-kinase; PLCβ4, phospholipase C β4; PKC, protein kinase C; PPD, paired-pulse depression; PPF, paired-pulse facilitation; PTEN, phosphatase and tensin homolog; PC, Purkinje cell; RAbKO, raptor brain knockout; raptor, regulatory-associated

protein of mTOR; RAPuKO, raptor Purkinje cell knockout; rictor, rapamycin-insensitive companion of mTOR; RIPuKO, rictor Purkinje cell knockout; SGK1, serum-and glucocorticoid-induced protein kinase 1; (p)S6, (phosphorylated) ribosomal protein S6; TSC1/2, tuberous sclerosis complex 1/2; TSCPuKO, TSC1 Purkinje cell knockout.

REFERENCES

Angliker, N. & Ruegg, M.A. (2013) In vivo evidence for mTORC2-mediated actin cytoskeleton rearrangement in neurons. *Bioarchitecture*, **3**, 113-118.

Arimura, N. & Kaibuchi, K. (2007) Neuronal polarity: from extracellular signals to intracellular mechanisms. *Nat Rev Neurosci*, **8**, 194-205.

Bajaj, N.P. & Miller, C.C. (1997) Phosphorylation of neurofilament heavy-chain side-arm fragments by cyclin-dependent kinase-5 and glycogen synthase kinase-3alpha in transfected cells. *J Neurochem*, **69**, 737-743.

Barmack, N.H., Qian, Z. & Yoshimura, J. (2000) Regional and cellular distribution of protein kinase C in rat cerebellar Purkinje cells. *J Comp Neurol*, **427**, 235-254.

Bentzinger, C.F., Romanino, K., Cloetta, D., Lin, S., Mascarenhas, J.B., Oliveri, F., Xia, J., Casanova, E., Costa, C.F., Brink, M., Zorzato, F., Hall, M.N. & Ruegg, M.A. (2008) Skeletal muscle-specific ablation of raptor, but not of rictor, causes metabolic changes and results in muscle dystrophy. *Cell Metab*, **8**, 411-424.

Briatore, F., Patrizi, A., Viltono, L., Sassoe-Pognetto, M. & Wulff, P. (2010) Quantitative organization of GABAergic synapses in the molecular layer of the mouse cerebellar cortex. *PLoS One*, **5**, e12119.

Carson, R.P., Van Nielen, D.L., Winzenburger, P.A. & Ess, K.C. (2012) Neuronal and glia abnormalities in Tsc1-deficient forebrain and partial rescue by rapamycin. *Neurobiol Dis*, **45**, 369-380.

Castets, P., Lin, S., Rion, N., Di Fulvio, S., Romanino, K., Guridi, M., Frank, S., Tintignac, L.A., Sinnreich, M. & Ruegg, M.A. (2013) Sustained activation of mTORC1 in skeletal muscle inhibits constitutive and starvation-induced autophagy and causes a severe, late-onset myopathy. *Cell Metab*, **17**, 731-744.

Chen, C., Kano, M., Abeliovich, A., Chen, L., Bao, S., Kim, J.J., Hashimoto, K., Thompson, R.F. & Tonegawa, S. (1995) Impaired motor coordination correlates with persistent multiple climbing fiber innervation in PKC gamma mutant mice. *Cell*, **83**, 1233-1242.

Ching, G.Y., Chien, C.L., Flores, R. & Liem, R.K. (1999) Overexpression of alpha-internexin causes abnormal neurofilamentous accumulations and motor coordination deficits in transgenic mice. *J Neurosci*, **19**, 2974-2986.

Cloetta, D., Thomanetz, V., Baranek, C., Lustenberger, R.M., Lin, S., Oliveri, F., Atanasoski, S. & Ruegg, M.A. (2013) Inactivation of mTORC1 in the developing brain causes microcephaly and affects gliogenesis. *J Neurosci*, **33**, 7799-7810.

Costa-Mattioli, M. & Monteggia, L.M. (2013) mTOR complexes in neurodevelopmental and neuropsychiatric disorders. *Nat Neurosci*, **16**, 1537-1543.

Cross, D.A., Alessi, D.R., Cohen, P., Andjelkovich, M. & Hemmings, B.A. (1995) Inhibition of glycogen synthase kinase-3 by insulin mediated by protein kinase B. *Nature*, **378**, 785-789.

Curatolo, P., Bombardieri, R. & Jozwiak, S. (2008) Tuberous sclerosis. *Lancet*, **372**, 657-668.

Demirkan, G., Yu, K., Boylan, J.M., Salomon, A.R. & Gruppuso, P.A. (2011) Phosphoproteomic profiling of in vivo signaling in liver by the mammalian target of rapamycin complex 1 (mTORC1). *PLoS One*, **6**, e21729.

Fritschy, J.M., Panzanelli, P., Kralic, J.E., Vogt, K.E. & Sassoe-Pognetto, M. (2006) Differential dependence of axo-dendritic and axo-somatic GABAergic synapses on GABAA receptors containing the alpha1 subunit in Purkinje cells. *J Neurosci*, **26**, 3245-3255.

Garrett, A.M., Schreiner, D., Lobas, M.A. & Weiner, J.A. (2012) gamma-protocadherins control cortical dendrite arborization by regulating the activity of a FAK/PKC/MARCKS signaling pathway. *Neuron*, **74**, 269-276.

Gibson, D.A., Tymanskyj, S., Yuan, R.C., Leung, H.C., Lefebvre, J.L., Sanes, J.R., Chedotal, A. & Ma, L. (2014) Dendrite self-avoidance requires cell-autonomous slit/robo signaling in cerebellar purkinje cells. *Neuron*, **81**, 1040-1056.

Goto, J., Talos, D.M., Klein, P., Qin, W., Chekaluk, Y.I., Anderl, S., Malinowska, I.A., Di Nardo, A., Bronson, R.T., Chan, J.A., Vinters, H.V., Kernie, S.G., Jensen, F.E., Sahin, M. & Kwiatkowski, D.J. (2011) Regulable neural progenitor-specific Tsc1 loss yields giant cells with organellar dysfunction in a model of tuberous sclerosis complex. *Proc Natl Acad Sci U S A*, **108**, E1070-1079.

Gown, A.M. & Willingham, M.C. (2002) Improved detection of apoptotic cells in archival paraffin sections: immunohistochemistry using antibodies to cleaved caspase 3. *J Histochem Cytochem*, **50**, 449-454.

Hashimoto, K. & Kano, M. (2013) Synapse elimination in the developing cerebellum. *Cell Mol Life Sci*, **70**, 4667-4680.

Hirano, T. (2013) Long-term depression and other synaptic plasticity in the cerebellum. *Proc Jpn Acad Ser B Phys Biol Sci*, **89**, 183-195.

Holmgren, A., Bouhy, D. & Timmerman, V. (2012) Neurofilament phosphorylation and their proline-directed kinases in health and disease. *J Peripher Nerv Syst*, **17**, 365-376.

Huang, W., Zhu, P.J., Zhang, S., Zhou, H., Stoica, L., Galiano, M., Krnjevic, K., Roman, G. & Costa-Mattioli, M. (2013) mTORC2 controls actin polymerization required for consolidation of long-term memory. *Nat Neurosci*, **16**, 441-448.

Ichise, T., Kano, M., Hashimoto, K., Yanagihara, D., Nakao, K., Shigemoto, R., Katsuki, M. & Aiba, A. (2000) mGluR1 in cerebellar Purkinje cells essential for long-term depression, synapse elimination, and motor coordination. *Science*, **288**, 1832-1835.

Kakegawa, W., Miyoshi, Y., Hamase, K., Matsuda, S., Matsuda, K., Kohda, K., Emi, K., Motohashi, J., Konno, R., Zaitsu, K. & Yuzaki, M. (2011) D-serine regulates cerebellar LTD and motor coordination through the delta2 glutamate receptor. *Nat Neurosci*, **14**, 603-611.

Kakizawa, S., Yamasaki, M., Watanabe, M. & Kano, M. (2000) Critical period for activity-dependent synapse elimination in developing cerebellum. *J Neurosci*, **20**, 4954-4961.

Kano, M., Hashimoto, K., Chen, C., Abeliovich, A., Aiba, A., Kurihara, H., Watanabe, M., Inoue, Y. & Tonegawa, S. (1995) Impaired synapse elimination during cerebellar development in PKC gamma mutant mice. *Cell*, **83**, 1223-1231.

Kano, M., Hashimoto, K. & Tabata, T. (2008) Type-1 metabotropic glutamate receptor in cerebellar Purkinje cells: a key molecule responsible for long-term depression, endocannabinoid signalling and synapse elimination. *Philos Trans R Soc Lond B Biol Sci*, **363**, 2173-2186.

Kano, M., Hashimoto, K., Watanabe, M., Kurihara, H., Offermanns, S., Jiang, H., Wu, Y., Jun, K., Shin, H.S., Inoue, Y., Simon, M.I. & Wu, D. (1998) Phospholipase cbeta4 is specifically involved in climbing fiber synapse elimination in the developing cerebellum. *Proc Natl Acad Sci U S A*, **95**, 15724-15729.

Kwiatkowski, D.J., Zhang, H., Bandura, J.L., Heiberger, K.M., Glogauer, M., el-Hashemite, N. & Onda, H. (2002) A mouse model of TSC1 reveals sex-dependent lethality from liver hemangiomas, and up-regulation of p70S6 kinase activity in Tsc1 null cells. *Hum Mol Genet*, **11**, 525-534.

Kwon, C.H., Luikart, B.W., Powell, C.M., Zhou, J., Matheny, S.A., Zhang, W., Li, Y., Baker, S.J. & Parada, L.F. (2006) Pten regulates neuronal arborization and social interaction in mice. *Neuron*, **50**, 377-388.

Laplante, M. & Sabatini, D.M. (2012) mTOR Signaling. *Cold Spring Harb Perspect Biol*, **4**.

Lefebvre, J.L., Kostadinov, D., Chen, W.V., Maniatis, T. & Sanes, J.R. (2012) Protocadherins mediate dendritic self-avoidance in the mammalian nervous system. *Nature*, **488**, 517-521.

Lipton, J.O. & Sahin, M. (2014) The neurology of mTOR. *Neuron*, **84**, 275-291.

Louis, E.D., Yi, H., Erickson-Davis, C., Vonsattel, J.P. & Faust, P.L. (2009) Structural study of Purkinje cell axonal torpedoes in essential tremor. *Neurosci Lett*, **450**, 287-291.

McDonald, B.J. & Moss, S.J. (1997) Conserved phosphorylation of the intracellular domains of GABA(A) receptor beta2 and beta3 subunits by cAMP-dependent protein kinase, cGMP-dependent protein kinase protein kinase C and Ca2+/calmodulin type II-dependent protein kinase. *Neuropharmacology*, **36**, 1377-1385.

Meikle, L., Pollizzi, K., Egnor, A., Kramvis, I., Lane, H., Sahin, M. & Kwiatkowski, D.J. (2008) Response of a neuronal model of tuberous sclerosis to mammalian target of rapamycin (mTOR) inhibitors: effects on mTORC1 and Akt signaling lead to improved survival and function. *J Neurosci*, **28**, 5422-5432.

Naska, S., Park, K.J., Hannigan, G.E., Dedhar, S., Miller, F.D. & Kaplan, D.R. (2006) An essential role for the integrin-linked kinase-glycogen synthase kinase-3 beta pathway during dendrite initiation and growth. *J Neurosci*, **26**, 13344-13356.

Notter, T., Panzanelli, P., Pfister, S., Mircsof, D. & Fritschy, J.M. (2014) A protocol for concurrent high-quality immunohistochemical and biochemical analyses in adult mouse central nervous system. *Eur J Neurosci*, **39**, 165-175.

Offermanns, S., Hashimoto, K., Watanabe, M., Sun, W., Kurihara, H., Thompson, R.F., Inoue, Y., Kano, M. & Simon, M.I. (1997) Impaired motor coordination and persistent multiple climbing fiber innervation of cerebellar Purkinje cells in mice lacking Galphaq. *Proc Natl Acad Sci U S A*, **94**, 14089-14094.

Oh, W.J. & Jacinto, E. (2011) mTOR complex 2 signaling and functions. *Cell Cycle*, **10**, 2305-2316.

Patrizi, A., Scelfo, B., Viltono, L., Briatore, F., Fukaya, M., Watanabe, M., Strata, P., Varoqueaux, F., Brose, N., Fritschy, J.M. & Sassoe-Pognetto, M. (2008) Synapse formation and clustering of neuroligin-2 in the absence of GABAA receptors. *Proc Natl Acad Sci U S A*, **105**, 13151-13156.

Pekny, M. & Nilsson, M. (2005) Astrocyte activation and reactive gliosis. *Glia*, **50**, 427-434.

Reith, R.M., McKenna, J., Wu, H., Hashmi, S.S., Cho, S.H., Dash, P.K. & Gambello, M.J. (2013) Loss of Tsc2 in Purkinje cells is associated with autistic-like behavior in a mouse model of tuberous sclerosis complex. *Neurobiol Dis*, **51**, 93-103.

Robertson, J.D., Orrenius, S. & Zhivotovsky, B. (2000) Review: nuclear events in apoptosis. *J Struct Biol*, **129**, 346-358.

Saito, H., Tsumura, H., Otake, S., Nishida, A., Furukawa, T. & Suzuki, N. (2005) L7/Pcp-2-specific expression of Cre recombinase using knock-in approach. *Biochem Biophys Res Commun*, **331**, 1216-1221.

Santini, E. & Klann, E. (2011) Dysregulated mTORC1-Dependent Translational Control: From Brain Disorders to Psychoactive Drugs. *Front Behav Neurosci*, **5**, 76.

Sarbassov, D.D., Ali, S.M., Sengupta, S., Sheen, J.H., Hsu, P.P., Bagley, A.F., Markhard, A.L. & Sabatini, D.M. (2006) Prolonged rapamycin treatment inhibits mTORC2 assembly and Akt/PKB. *Mol Cell*, **22**, 159-168.

Sasaki, T., Ishiguro, K. & Hisanaga, S. (2009) Novel axonal distribution of neurofilament-H phosphorylated at the glycogen synthase kinase 3beta-phosphorylation site in its E-segment. *J Neurosci Res*, **87**, 3088-3097.

Sasaki, T., Taoka, M., Ishiguro, K., Uchida, A., Saito, T., Isobe, T. & Hisanaga, S. (2002) In vivo and in vitro phosphorylation at Ser-493 in the glutamate (E)-segment of neurofilament-H subunit by glycogen synthase kinase 3beta. *J Biol Chem*, **277**, 36032-36039.

Schmahmann, J.D., Weilburg, J.B. & Sherman, J.C. (2007) The neuropsychiatry of the cerebellum - insights from the clinic. *Cerebellum*, **6**, 254-267.

Schmued, L.C. & Hopkins, K.J. (2000) Fluoro-Jade B: a high affinity fluorescent marker for the localization of neuronal degeneration. *Brain Res*, **874**, 123-130.

Schneider Gasser, E.M., Straub, C.J., Panzanelli, P., Weinmann, O., Sassoe-Pognetto, M. & Fritschy, J.M. (2006) Immunofluorescence in brain sections: simultaneous detection of presynaptic and postsynaptic proteins in identified neurons. *Nat Protoc*, **1**, 1887-1897.

Shea, T.B., Chan, W.K., Kushkuley, J. & Lee, S. (2009) Organizational dynamics, functions, and pathobiological dysfunctions of neurofilaments. *Results Probl Cell Differ*, **48**, 29-45.

Shimobayashi, M. & Hall, M.N. (2014) Making new contacts: the mTOR network in metabolism and signalling crosstalk. *Nat Rev Mol Cell Biol*, **15**, 155-162.

Silverman, J.L., Yang, M., Lord, C. & Crawley, J.N. (2010) Behavioural phenotyping assays for mouse models of autism. *Nat Rev Neurosci*, **11**, 490-502.

Sotelo, C. & Dusart, I. (2009) Intrinsic versus extrinsic determinants during the development of Purkinje cell dendrites. *Neuroscience*, **162**, 589-600.

Tchorz, J.S., Suply, T., Ksiazek, I., Giachino, C., Cloetta, D., Danzer, C.P., Doll, T., Isken, A., Lemaistre, M., Taylor, V., Bettler, B., Kinzel, B. & Mueller, M. (2012) A modified RMCE-compatible Rosa26 locus for the expression of transgenes from exogenous promoters. *PLoS One*, **7**, e30011.

Thomanetz, V., Angliker, N., Cloetta, D., Lustenberger, R.M., Schweighauser, M., Oliveri, F., Suzuki, N. & Ruegg, M.A. (2013) Ablation of the mTORC2 component rictor in brain or Purkinje cells affects size and neuron morphology. *J Cell Biol*, **201**, 293-308.

Tsai, P.T., Hull, C., Chu, Y., Greene-Colozzi, E., Sadowski, A.R., Leech, J.M., Steinberg, J., Crawley, J.N., Regehr, W.G. & Sahin, M. (2012) Autistic-like behaviour and cerebellar dysfunction in Purkinje cell Tsc1 mutant mice. *Nature*, **488**, 647-651.

Tyagarajan, S.K. & Fritschy, J.M. (2014) Gephyrin: a master regulator of neuronal function? *Nat Rev Neurosci*, **15**, 141-156.

Um, S.H., Frigerio, F., Watanabe, M., Picard, F., Joaquin, M., Sticker, M., Fumagalli, S., Allegrini, P.R., Kozma, S.C., Auwerx, J. & Thomas, G. (2004) Absence of S6K1 protects against age- and diet-induced obesity while enhancing insulin sensitivity. *Nature*, **431**, 200-205.

Viltono, L., Patrizi, A., Fritschy, J.M. & Sassoe-Pognetto, M. (2008) Synaptogenesis in the cerebellar cortex: differential regulation of gephyrin and GABAA receptors at somatic and dendritic synapses of Purkinje cells. *J Comp Neurol*, **508**, 579-591.

Wang, Q., Liu, L., Pei, L., Ju, W., Ahmadian, G., Lu, J., Wang, Y., Liu, F. & Wang, Y.T. (2003) Control of synaptic strength, a novel function of Akt. *Neuron*, **38**, 915-928.

Wang, S.S., Kloth, A.D. & Badura, A. (2014) The Cerebellum, Sensitive Periods, and Autism. *Neuron*, **83**, 518-532.

Watanabe, M. & Kano, M. (2011) Climbing fiber synapse elimination in cerebellar Purkinje cells. *Eur J Neurosci*, **34**, 1697-1710.

Watanabe, S., Endo, S., Oshima, E., Hoshi, T., Higashi, H., Yamada, K., Tohyama, K., Yamashita, T. & Hirabayashi, Y. (2010) Glycosphingolipid synthesis in cerebellar Purkinje neurons: roles in myelin formation and axonal homeostasis. *Glia*, **58**, 1197-1207.

Wierenga, C.J., Becker, N. & Bonhoeffer, T. (2008) GABAergic synapses are formed without the involvement of dendritic protrusions. *Nat. Neurosci.*, **11**, 1044-1052.

Wuchter, J., Beuter, S., Treindl, F., Herrmann, T., Zeck, G., Templin, M.F. & Volkmer, H. (2012) A comprehensive small interfering RNA screen identifies signaling pathways required for gephyrin clustering. *J Neurosci*, **32**, 14821-14834.

Wullschleger, S., Loewith, R. & Hall, M.N. (2006) TOR signaling in growth and metabolism. *Cell*, **124**, 471-484.

Yamada, K. & Watanabe, M. (2002) Cytodifferentiation of Bergmann glia and its relationship with Purkinje cells. *Anat Sci Int*, **77**, 94-108.

Yang, M. & Crawley, J.N. (2009) Simple behavioral assessment of mouse olfaction. *Curr Protoc Neurosci*, **Chapter 8**, Unit 8 24.

Yang, Y., Coleman, M., Zhang, L., Zheng, X. & Yue, Z. (2013) Autophagy in axonal and dendritic degeneration. *Trends Neurosci*, **36**, 418-428.

TABLES

	mouse line	1st Ampl (in pA)	2nd Ampl (in pA)	PPD/PPF (% of 1st Ampl)	10-90% rise time (in ms)	10-90% rise slope (in pA/ms)	decay time constant (in ms)	cells (n)
CF-EPSC	Control RAPuKO	-1275 ± 55	-871 ± 39	68 ± 1	0.67 ± 0.03	-1779 ± 128	19.6 ± 1.2	15
	RAPuKO	-965 ± 42 t_{31}= 4.5 P < 0.0001	-565 ±23 t_{31} = 7.1 P < 0.0001	59 ± 2 *** t_{31} = 4.5 P < 0.0001	0.77 ± 0.04 t_{29} = 2.03 P = 0.052	-1131 ± 85 t_{29} = 4.3 P = 0.0002	11.7 ± 0.5 t_{31} = 6.4 P = < 0.0001	≥ 16
	Control RIPuKO	-1150 ± 68	-790 ± 44	69 ± 2	0.66 ± 0.03	-1606 ± 116	18.9 ± 1.1	≥ 10
	RIPuKO	-944 ± 67 t_{27} = 2.02 P = 0.053	-512 ± 37 t_{27} = 4.7 P < 0.0001	55 ± 2 t_{27} = 6.1 P < 0.0001	0.83 ± 0.06 t_{23} = 2.3 P = 0.031	-1118 ± 126 t_{23} = 2.7 P = 0.014	10.2 ± 0.6 t_{26} =7.8 P < 0.0001	≥ 15
PF-EPSC	Control RIPuKO	-229 ± 12	-317 ± 26	140 ± 8	2.32 ± 0.18	-91 ± 8	11.6 ± 0.7	6
	RIPuKO	-266 ± 26 t_{12} = 1.15 P = 0.27	-338 ± 47 t_{12} = 0.35 P = 0.73	133 ± 2 t_{12} = 1.1 P = 0.29	1.79 ± 0.05 t_{12} = 3.2 P = 0.007	-138 ± 19 t_{12} = 2.02 P = 0.067	8.7 ± 0.4 t_{13} = 4.3 P = 0.0009	≥ 8

Table 1: Kinetics and short-term plasticity of CF-EPSCs and PF-EPSCs. Average values ± SEM are indicated. A two-tailed Student's *t*-test was used to compare knockout mice with corresponding control mice.

		RIPuKO	RAPuKO
Behaviour	Motor coordination	Deficits already at young age	Deficits only at high age
	Olfactory habituation /dishabituation	Normal	Interest in social odours reduced
Morphology	Purkinje soma size	Reduced by ~ 25%*	Reduced by ~ 50%
	Dendritic tree	~ 40% of PCs multiple primary dendrites (up to 4)*	~ 40% of PCs multiple primary dendrites (up to 6)
Electrophysiology	Capacitance	Reduced by ~ 30%	Reduced by ~ 70%
	mEPSC	Frequency reduced by ~ 50%*	Normal
	mIPSC	Amplitude reduced by ~ 15 %*	Frequency reduced by ~ 80%
	Climbing fibre innervation	~ 40% of PCs multiple CFs	Normal
PC survival	Purkinje cell density	Normal (analysed up to 90 wk)	Reduced in mice >11 wk
	Purkinje cell apoptosis	no	yes

* see Thomanetz *et al.*, 2013

Table 2: Comparison of phenotypes of RIPuKO and RAPuKO mice.

FIGURE LEGENDS

Figure 1: Behavioural assessment of RIPuKO and RAPuKO mice. ***A*** and ***B***, Balance beam tests of RIPuKO (*A*) and RAPuKO (*B*) mice and their respective control littermates at different ages. The number of hind leg slips per meter was measured as a readout of ataxia. For each group n ≥ 8 mice were tested. ***C*** and ***D***, Footprint pattern analysis of RIPuKO (*C*) and RAPuKO (*D*) mice and their control mice (n ≥ 7 mice for each group) of the indicated age. The steps of the hind and front paws are indicated in black and red, respectively. Hind limb gait width (W) was measured as indicated in (*C*). ***E*** and ***F***, Olfactory habituation/dishabituation test with n ≥ 12 male RIPuKO (*E*) or RAPuKO (*F*) mice and corresponding control mice. Non-social and social odours were presented to the mice on a cotton swab in 2 and 3 repetitions as indicated. Bars represent mean ± SEM. Data of (*A* – *D*) were analysed by a two-tailed Student's *t*-test and for (*E* – *F*) a two-way ANOVA, Bonferroni's post hoc analysis was used. *P*-values: ** $P < 0.01$; * $P < 0.05$; ns $P \geq 0.05$. Scale bar: 10 cm.

Figure 2. Morphology of Purkinje cells is altered in RAPuKO mice. ***A***, Sagittal cerebellar slices of 6-week-old RAPuKO mice and corresponding control mice were co-stained for calbindin (red) and pS6 (green). All calbindin-positive neurons are also pS6-positive (yellow) in control mice (left) whereas most Purkinje cells are pS6-negative in RAPuKO mice (right). ***B***, Average soma area of Purkinje cells of control mice (black bars) and pS6-positive (yellow) or pS6-negative (red) Purkinje cells in RAPuKO mice of different age. Data represent Purkinje cell somata of lobes IV & V of n ≥ 3 mice for each time point and genotype. ***C***, Purkinje cells of 4- to 6-week-old RAPuKO or control mice (n ≥ 8) were labelled with biocytin by the whole-cell patch clamp technique and detected by fluorescein (DTAF)

streptavidin after PFA fixation. Pictures in (*C*) represent the projection of 52 or 28 confocal optical sections (voxel size: 0.27 x 0.27 x 0.5 μm) taken from a control or a RAPuKO mouse, respectively. ***D***, Quantification of the number of primary dendrites originating from a Purkinje cell soma. ***E***, Cerebellar slices of the mice described in (*A*) were co-stained for calbindin (red) and the mTORC2 downstream target PKCγ (green). Purkinje cells of RAPuKO and control mice show similar levels of PKCγ. Bars represent mean ± SEM. Statistical analysis used one-way ANOVA with Tukey's post hoc analysis. *P*-values: *** $P < 0.001$; ** $P < 0.01$; ns $P \geq 0.05$. Scale bars: 200 μm (*A* and *E*), 50 μm (*C*).

Figure 3. Inhibitory synaptic input is altered in raptor-knockout Purkinje cells. ***A***, Sample traces of mEPSC recordings taken from Purkinje cells of 6-week-old control or RAPuKO mice. ***B*** and ***C***, Quantification of mEPSC frequency (*B*) and amplitude (*C*) recorded from 5 RAPuKO (red) and 4 control (black) mice. Mean values and cumulative distributions of recordings from 12 raptor-deficient (red) and 14 control (black) Purkinje cells are shown. ***D***, mIPSC sample traces of Purkinje cells of 6-week-old control or RAPuKO mice. ***E*** and ***F***, Quantification of mIPSC frequency (*E*) and amplitude (*F*) recorded from 3 RAPuKO (red) and 3 control (black) mice. Mean values and cumulative distributions of recordings from 14 raptor-deficient (red) and 16 control (black) Purkinje cells are shown. ***G***, Sagittal cerebellar sections of 6-week-old RAPuKO or control mice stained with antibodies to the α1 subunit of $GABA_A$ receptors (red). Co-staining against Car8 (green) and pS6 (blue) was used to identify Purkinje cell somata and to confirm raptor deficiency, respectively. Each picture shows projections of 3 confocal optical sections (voxel size: 0.13 x 0.13 x 0.44 μm). ***H***, Staining of the molecular layer of the same mice used in (*G*) for $GABA_A$ α1 (red), GAD65 (green; stains GABAergic presynaptic terminals) and for pS6 (blue). Each picture shows projections of 3 confocal optical sections (voxel size: 0.1 x 0.1 x 0.44 μm). ***I*** and ***K***, Analysis of the

perisomatic $GABA_A$ α1 subunit clusters shown in (*G*). (*I*) shows the average number of $GABA_A$ α1 subunit clusters at the soma of pS6-negative Purkinje cells (n ≥ 5 per mouse) of RAPuKO mice (n = 6) or Purkinje cells (n ≥ 10 per mouse) of control mice (n = 4). (*K*) shows the quantification of the $GABA_A$ α1 subunit cluster size at these somata. ***J*** and ***L***, Quantification of the mean density (*J*) or size (*L*) of the clusters positive for GAD65, for the $GABA_A$ α1 subunit (α1) and for both (GAD65 + α1), detected in the molecular layer of control (black) or RAPuKO (red) mice (n ≥ 4 per genotype). Bars represent mean ± SEM. Data in *B, C, E, F* and *I - L* were analysed by a two-tailed Student's *t*-test. *P*-values: *** $P < 0.001$; ** $P < 0.01$; ns $P \geq 0.05$. Scale bars: 10 μm (*G*) and 20 μm (*H*).

Figure 4. Rictor-deficient Purkinje cells are innervated by multiple CFs, show impairment in dendritic self-avoidance but normal LTD. ***A*** - ***C***, Paired current pulses in the granule cell layer were used to elicit CF-EPSC responses in Purkinje cells. Stimulation intensity was continuously increased and the size of the postsynaptic response was recorded. In control mice (*A*), the CF-EPSC response occurred in an "all or nothing" manner and did not change by further increasing the stimulation intensity, indicating mono CF innervation of the Purkinje cell. In 4-week-old RIPuKO (*B*) or 12-week-old RIPuKO mice (*C*), CF-EPSC responses revealed 2 or 3 discrete steps in response to increasing stimulation intensity, indicating multiple innervation by CFs. ***D***, Percentage of the Purkinje cells showing the indicated number of discrete CF-EPSC steps of 4- or 12-week-old RIPuKO or corresponding control mice. The indicated numbers of Purkinje cells were analysed from n ≥ 4 mice for each genotype and age. ***E*** - ***G***, Analysis of CF innervation of Purkinje cells of 4-week-old RAPuKO or control mice (n ≥ 4) using the same experimental approach as described in (*A - D*). ***H***, Stimulation paradigm to elicit cerebellar LTD by repetitive stimulation of afferent PFs and simultaneous depolarization of the voltage-clamped Purkinje cell to 20 mV for 500 ms. ***I***

and ***J***, Sample traces of PF-EPSCs recorded in Purkinje cells of a 7-week-old control (*I*) or RIPuKO mouse (*J*) before and 30 minutes after LTD induction. ***K***, Fold change of the PF-EPSC amplitude monitored in 6 control and 11 rictor-deficient Purkinje cells over 40 minutes after LTD induction ($n \geq 3$ individual mice of each genotype). There is no difference between control- and rictor-deficient neurons. ***L*** and ***M***, Confocal microscopy pictures of spiny distal dendritic branches of biocytin-labelled Purkinje cells of 12-week-old control or RIPuKO mice. Acute slices containing the labelled cells were re-sliced and stained with Cy3-streptdavidin (red) and an anti-PKCγ antibody (blue) to detect the labelled cells and to confirm mTORC2 ablation, respectively, as previously described (Thomanetz *et al.*, 2013). Pictures represent projections of 81 or 93 confocal optical sections (voxel size: 0.07 x 0.07 x 0.2 μm) taken from a control or a RIPuKO mouse, respectively. The number of dendritic self-crossings (white arrows) was counted. ***N***, Relative number of dendritic self-crossings detected in RIPuKO mice expressed as percentage of dendritic self-crossings detected in control mice. $n \geq 30$ Purkinje cells of RIPuKO or corresponding control mice ($n = 4$ for each genotype) were analysed. Data in (*K* and *N*) represent mean ± SEM and were analysed by a two-tailed Student's *t*-test. *P*-values: *** $P < 0.001$. Scale bars: 25 μm (*L* and *M*).

Figure 5. Depletion of raptor, but not rictor causes age-dependent loss of Purkinje cells due to apoptosis. ***A***, Sagittal cerebellar slices of 86-week-old RIPuKO mice and corresponding control mice were co-stained for calbindin (red) and PKCγ (green) to confirm mTORC2 ablation in Purkinje cells. Calbindin staining was used to determine Purkinje cell density in the cerebellar lobes IV & V of RIPuKO and control mice. ***B***, Purkinje cell density determined for RIPuKO and corresponding control mice at different age. For each age and genotype, $n \geq 3$ mice were analysed with $n \geq 3$ cerebellar slices per mouse. ***C*** and ***D***, Staining for calbindin (red) and pS6 (green) to analyse Purkinje cell density and mTORC1 ablation in

41-week-old RAPuKO and control mice. Purkinje cell density at different age was monitored as described in (*A* and *B*). ***E***, Confocal pictures of an apoptotic Purkinje cell detected by co-staining of cerebellar slices of an 11-week-old RAPuKO mouse using Hoechst and antibodies against calbindin and CC3. Each picture shows the projection of 19 optical confocal sections (voxel size: 0.1 x 0.1 x 0.46 μm). ***F***, The fraction of cerebellar slices containing the indicated numbers of CC3-positive Purkinje cells were determined for RAPuKO or control mice (n = 4 mice per genotype). ***G***, GFAP staining of a sagittal cerebellar slice of an 11-week-old RAPuKO or control mouse. Similar results were obtained with additional RAPuKO and control mice of the same age (n = 3 mice per genotype). The inset highlights increased GFAP expression in palisade-like structures in RAPuKO mice (white arrow). IV - X indicate the numbers of the cerebellar lobes. ***H***, Cerebellar section of an 11-week-old RAPuKO mouse co-stained against GFAP, PKCγ and mouse-IgG followed by confocal microscopy analysis (voxel size: 0.34 x 0.34 x 0.54 μm). Projections of 25 confocal planes are shown. PKCγ labels Purkinje cells while mouse IgG stains blood vessels, which helps to differentiate between GFAP staining and blood vessels that are also seen in the insets of (*G*). Bars represent mean ± SEM. Data of (*B, D* and *F*) were analysed by a two-tailed Student's *t*-test. *P*-values: *** $P < 0.001$; ** $P < 0.01$; ns $P \geq 0.05$. Scale bars: 200 μm (*A* and *C*), 20 μm (*E*), 1 mm (*G*), 100 μm (inset of *G*), 50 μm (*H*). PCL: Purkinje cell layer; ML: molecular layer; GCL: granule cell layer.

Figure 6. Raptor-deficient Purkinje cells show dendritic degeneration and axonal swellings that accumulate neurofilaments. ***A***, Example of Fluoro-Jade B (FJB) puncta seen in the molecular layer (white arrow) and in the Purkinje cell layer (yellow arrow) of RAPuKO mice. For quantification shown in (*B*), accumulation of FJB-positive puncta were counted as one FJB patch (encircled with the dashed, pink line). ***B***, Fraction of cerebellar slices of 6- and

11-week-old RAPuKO or control mice (n = 3 for each age and genotype) that contain 0; 1-5; 6-10 or > 10 FJB patches. ***C***, Confocal picture of a biocytin-labelled Purkinje cell of a 6-week-old RAPuKO mouse that shows signs of atrophy and beadings (white arrows), indicative of dendritic degeneration. Projection of 52 confocal optical sections is shown (voxel size: 0.27 x 0.27 x 0.2 μm). ***D – G***, Confocal pictures of sagittal cerebellar slices of 11-week-old RAPuKO mice stained for calbindin and for neurofilament H (*D*), phosphorylated neurofilaments (SMI31) (*E*), cytochrome c (*F*), or synaptophysin (*G*). Axonal swellings (white arrows) contained neurofilament H and phosphorylated forms of neurofilaments (SMI31-positive) but were devoid of cytochrome c and synaptophysin. Projections of 33 – 84 confocal optical sections are shown (voxel size: 0.11 x 0.11 x 0.2 μm). ***H***, Relative proportion of cerebellar sections of 6- and 11-week-old RAPuKO or control mice (n = 4 mice per age and genotype) that reveal 0; 1-5 or > 5 axonal swellings proximal to the Purkinje cell somata as shown in (*D* - *G*). ***I***, Western blot analysis of total brain lysates derived from embryonic day 19.5 mice depleted of raptor as previously described (Cloetta *et al.*, 2013). Lysates were probed with a phospho-specific antibody recognizing P-Ser21 on GSK3α and P-Ser9 on GSK3β and antibodies recognizing the total protein. Antibodies to β-tubulin were used as loading control. ***J***, Quantification of Western blot signals shown in (*I*) relative to the intensities in control mice (n = 5 per genotype). Bars represent mean ± SEM. Data in (*B, H* and *J*) were analysed by a two-tailed Student's *t*-test. *P*-values: *** $P < 0.001$; ** $P < 0.01$; * $P < 0.05$; ns $P \geq 0.05$. Scale bars: 100 μm (*A*), 50 μm (*C*) and 25 μm (*D – G*). PCL: Purkinje cell layer; ML: molecular layer; GCL: granule cell layer.

Figure 7. Depletion of TSC1 in Purkinje cells results in the accumulation of neurofilaments in axons and in reactive gliosis. ***A*** and ***B***, Sagittal cerebellar slices of 11-week-old TSCPuKO mice were stained with anti-calbindin and anti-neurofilament H (*A*) or

SMI31 antibodies (*B*). Like in RAPuKO mice, axonal swellings (white arrows) that are positive for neurofilament H and phosphorylated neurofilaments (SMI31-positive) are detected in TSC1-deficient Purkinje cells. Pictures show projections of 100 (*A*) or 82 (*B*) confocal optical sections (voxel size: 0.27 x 0.27 x 0.2 μm). ***C***, Sagittal cerebellar slices of 11-week-old TSCPuKO or control mice stained for GFAP. The white arrow indicates reactive gliosis that manifests as palisade-like, GFAP-positive structures in the molecular layer of TSCPuKO but not control mice (n = 3 mice per genotype). Scale bars: 50 μm (*A* and *B*), 1 mm (*C*), 100 μm (inset of *C*). PCL: Purkinje cell layer; ML: molecular layer; GCL: granule cell layer. I to VIII designate numbers of the cerebellar lobes.

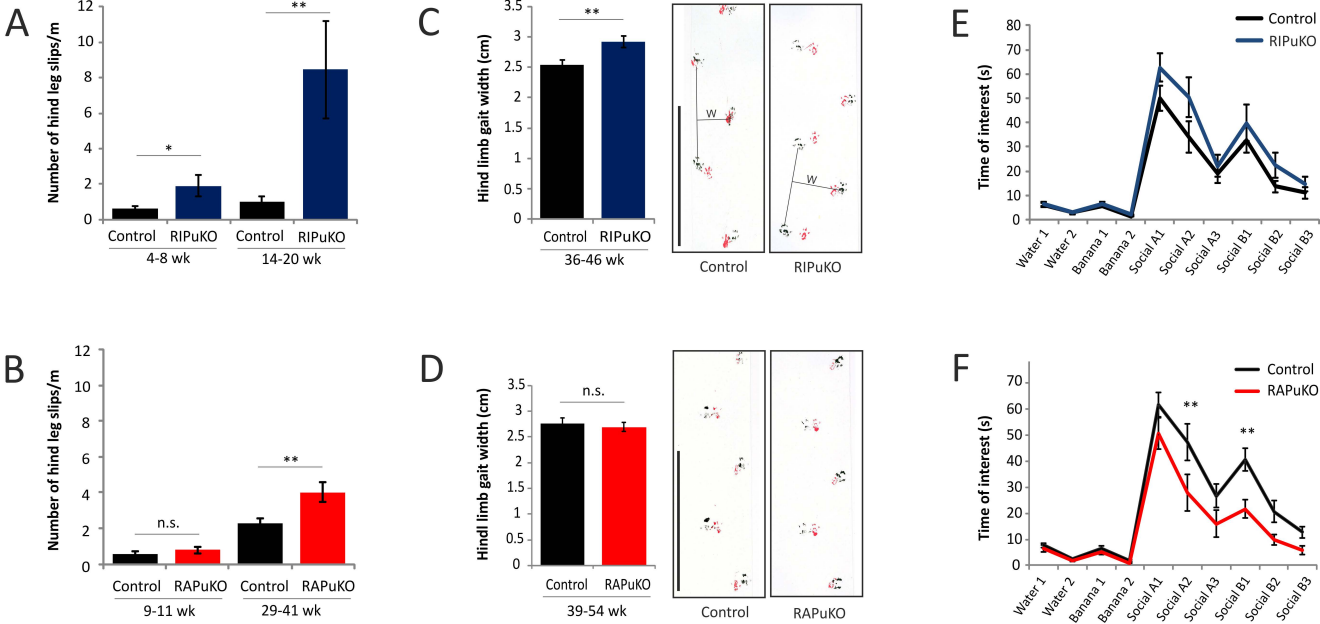
A
Number of hind leg slips/m
12
10
8
6
4
2
0
*
**
Control
RIPuKO
Control
RIPuKO
4-8 wk
14-20 wk
B
Number of hind leg slips/m
12
10
8
6
4
2
0
n.s.
**
Control
RAPuKO
Control
RAPuKO
9-11 wk
29-41 wk
C
Hind limb gait width (cm)
3.5
3
2.5
2
1.5
1
0.5
0
**
Control
RIPuKO
36-46 wk
W
W
Control
RIPuKO
D
Hindl limb gait width (cm)
3.5
3
2.5
2
1.5
1
0.5
0
n.s.
Control
RAPuKO
39-54 wk
Control
RAPuKO
E
Time of interest (s)
80
70
60
50
40
30
20
10
0
Control
RIPuKO
Water 1
Water 2
Banana 1
Banana 2
Social A1
Social A2
Social A3
Social B1
Social B2
Social B3
F
Time of interest (s)
70
60
50
40
30
20
10
0
Control
RAPuKO
**
**
Water 1
Water 2
Banana 1
Banana 2
Social A1
Social A2
Social A3
Social B1
Social B2
Social B3

Figure 1

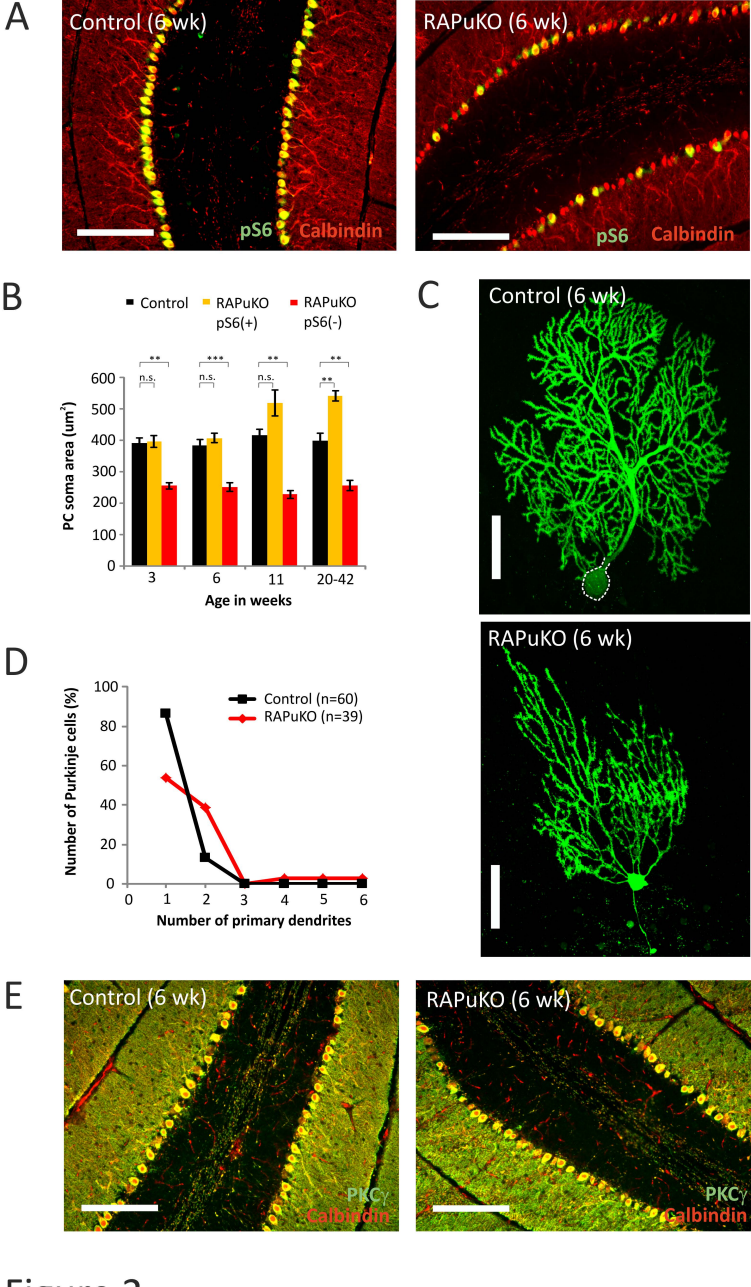
A
Control (6 wk)
pS6
Calbindin
RAPuKO (6 wk)
pS6
Calbindin
B
Control
RAPuKO pS6(+)
RAPuKO pS6(-)
PC soma area (um²)
600
500
400
300
200
100
0
n.s.
n.s.
n.s.
**
***
**
**
3
6
11
20-42
Age in weeks
C
Control (6 wk)
RAPuKO (6 wk)
D
Number of Purkinje cells (%)
100
80
60
40
20
0
Control (n=60)
RAPuKO (n=39)
0
1
2
3
4
5
6
Number of primary dendrites
E
Control (6 wk)
PKCγ
Calbindin
RAPuKO (6 wk)
PKCγ
Calbindin

Figure 2

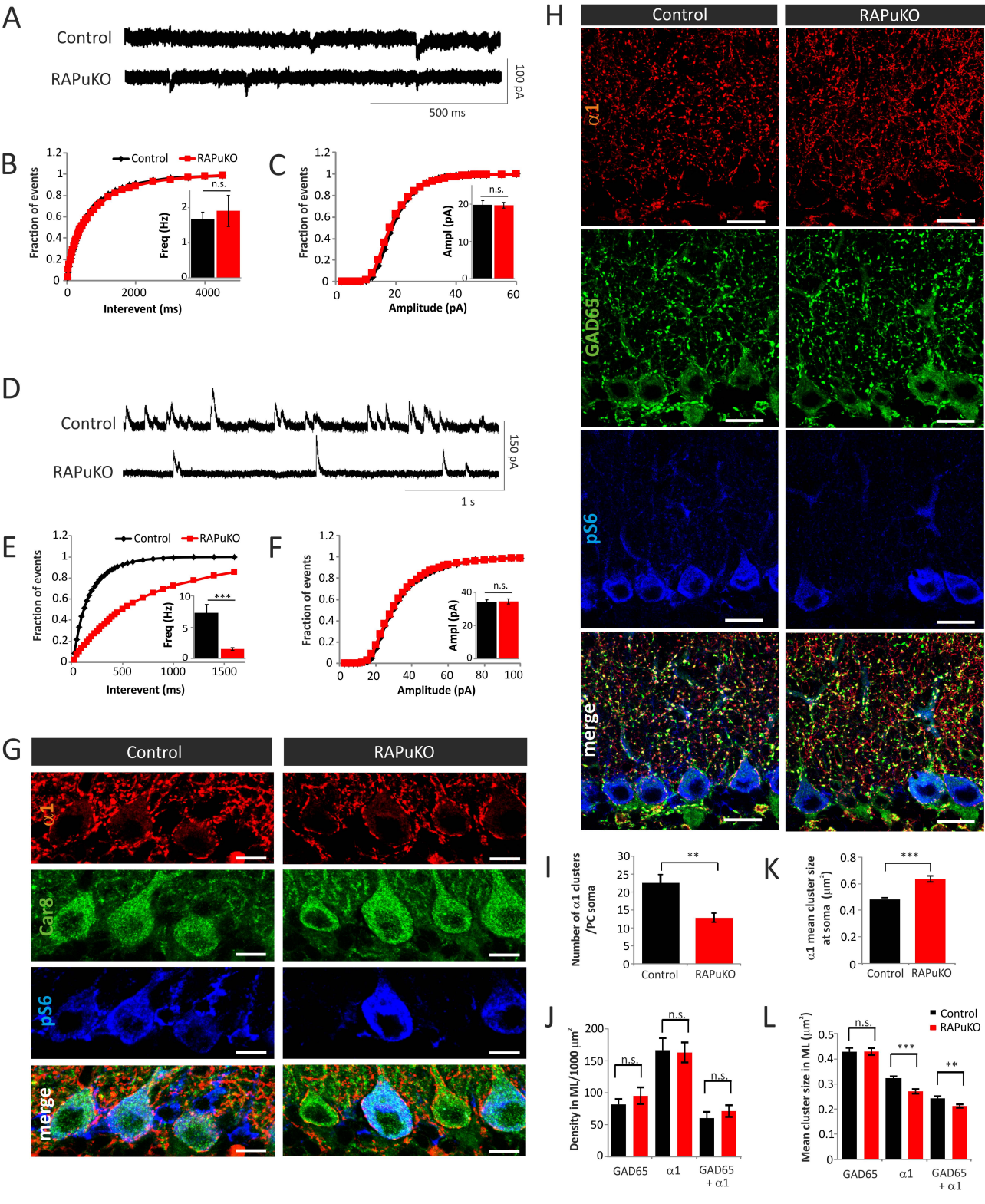
A
Control
RAPuKO
100 pA
500 ms
B
Control
RAPuKO
Fraction of events
Interevent (ms)
Freq (Hz)
n.s.
C
Fraction of events
Amplitude (pA)
Ampl (pA)
n.s.
D
Control
RAPuKO
150 pA
1 s
E
Control
RAPuKO
Fraction of events
Interevent (ms)
Freq (Hz)
***
F
Fraction of events
Amplitude (pA)
Ampl (pA)
n.s.
G
Control
RAPuKO
α1
Car8
pS6
merge
H
Control
RAPuKO
α1
GAD65
pS6
merge
I
Number of α1 clusters /PC soma
**
Control
RAPuKO
K
α1 mean cluster size at soma (μm²)
***
Control
RAPuKO
J
Density in ML/1000 μm²
n.s.
n.s.
n.s.
GAD65
α1
GAD65 + α1
L
Mean cluster size in ML (μm²)
Control
RAPuKO
n.s.
***
**
GAD65
α1
GAD65 + α1

Figure 3

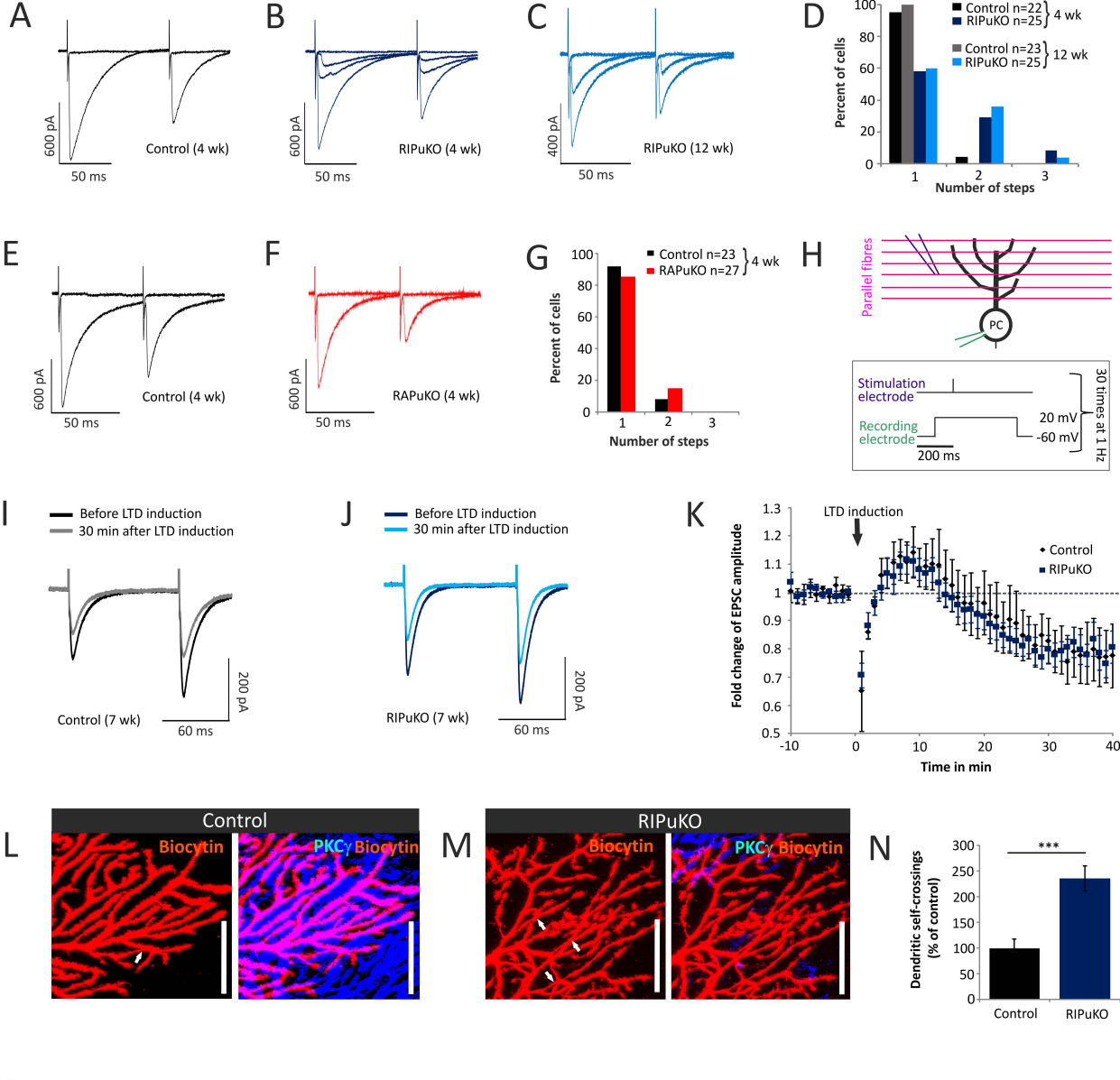
A
600 pA
50 ms
Control (4 wk)
B
600 pA
50 ms
RIPuKO (4 wk)
C
400 pA
50 ms
RIPuKO (12 wk)
D
Control n=22
RIPuKO n=25
4 wk
Control n=23
RIPuKO n=25
12 wk
Percent of cells
Number of steps
E
600 pA
50 ms
Control (4 wk)
F
600 pA
50 ms
RAPuKO (4 wk)
G
Control n=23
RAPuKO n=27
4 wk
Percent of cells
Number of steps
H
Parallel fibres
PC
Stimulation electrode
Recording electrode
20 mV
-60 mV
200 ms
30 times at 1 Hz
I
Before LTD induction
30 min after LTD induction
Control (7 wk)
200 pA
60 ms
J
Before LTD induction
30 min after LTD induction
RIPuKO (7 wk)
200 pA
60 ms
K
LTD induction
Control
RIPuKO
Fold change of EPSC amplitude
Time in min
L
Control
Biocytin
PKCγ Biocytin
M
RIPuKO
Biocytin
PKCγ Biocytin
N
***
Dendritic self-crossings (% of control)
Control
RIPuKO

Figure 4

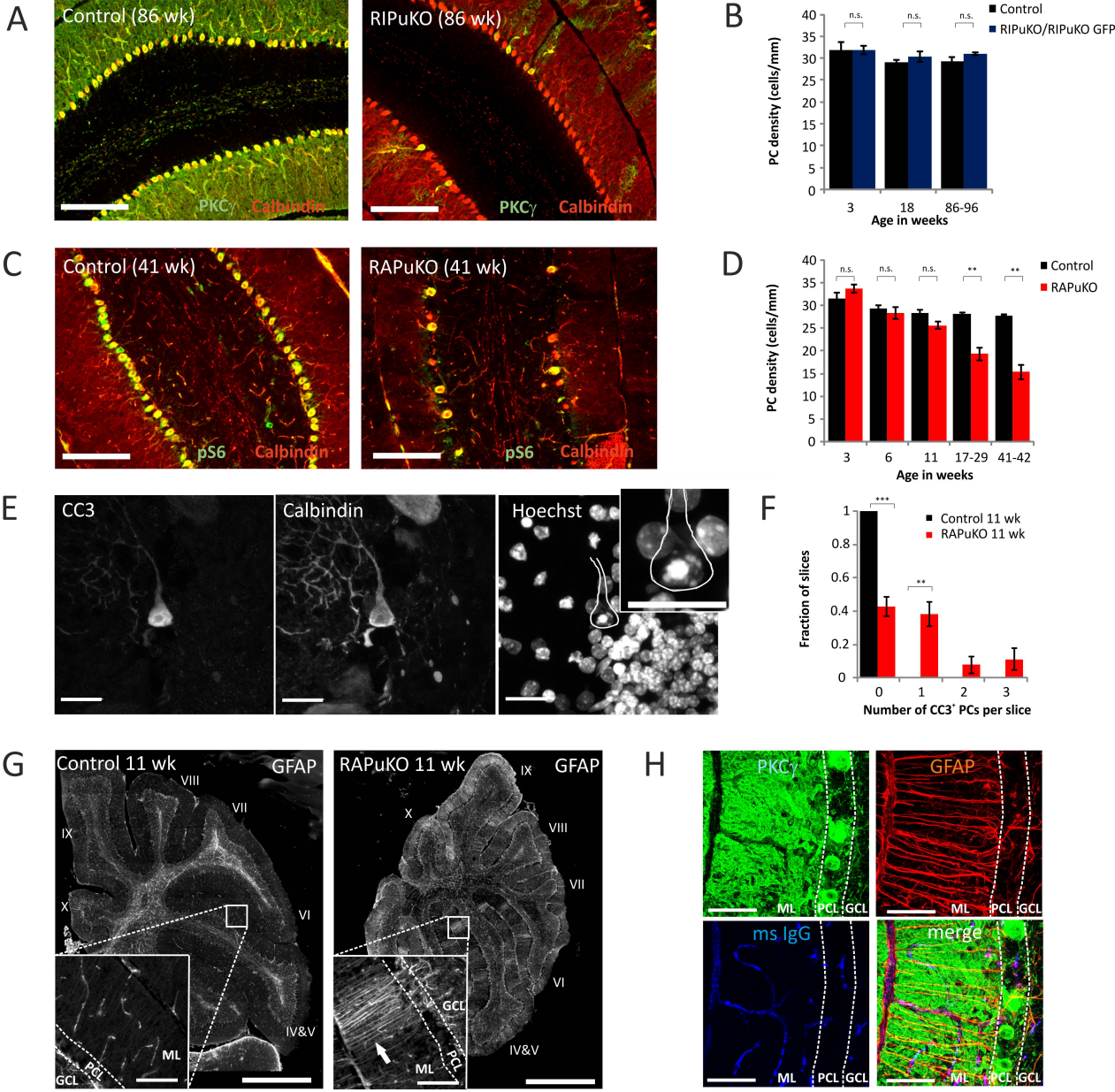
A
Control (86 wk)
PKCγ Calbindin
RIPuKO (86 wk)
PKCγ Calbindin
B
PC density (cells/mm)
n.s.
Control
RIPuKO/RIPuKO GFP
3
18
86-96
Age in weeks
C
Control (41 wk)
pS6 Calbindin
RAPuKO (41 wk)
pS6 Calbindin
D
PC density (cells/mm)
n.s.
**
Control
RAPuKO
3
6
11
17-29
41-42
Age in weeks
E
CC3
Calbindin
Hoechst
F
***
**
Control 11 wk
RAPuKO 11 wk
Fraction of slices
Number of CC3+ PCs per slice
G
Control 11 wk
GFAP
RAPuKO 11 wk
GFAP
ML
PCL
GCL
H
PKCγ
GFAP
ms IgG
merge
ML
PCL
GCL

Figure 5

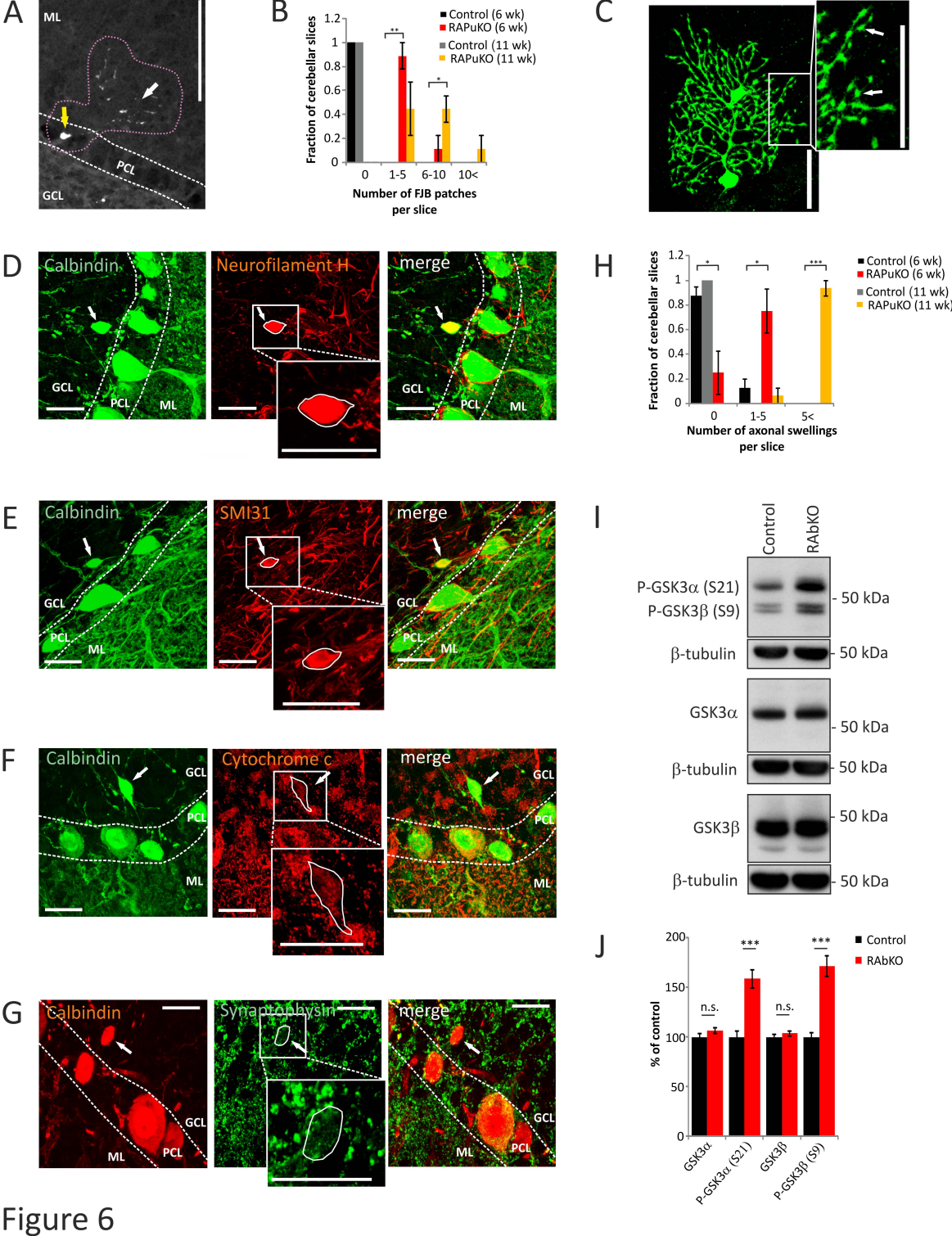
A
ML
PCL
GCL
B
Control (6 wk)
RAPuKO (6 wk)
Control (11 wk)
RAPuKO (11 wk)
Fraction of cerebellar slices
1.2
1
0.8
0.6
0.4
0.2
0
**
*
0
1-5
6-10
10<
Number of FJB patches per slice
C
D
Calbindin
Neurofilament H
merge
GCL
PCL
ML
H
Control (6 wk)
RAPuKO (6 wk)
Control (11 wk)
RAPuKO (11 wk)
Fraction of cerebellar slices
*
*
***
0
1-5
5<
Number of axonal swellings per slice
E
Calbindin
SMI31
merge
F
Calbindin
Cytochrome c
merge
I
Control
RAbKO
P-GSK3α (S21)
P-GSK3β (S9)
β-tubulin
GSK3α
GSK3β
50 kDa
G
Calbindin
Synaptophysin
merge
J
Control
RAbKO
% of control
200
150
100
50
0
n.s.
***
n.s.
***
GSK3α
P-GSK3α (S21)
GSK3β
P-GSK3β (S9)

Figure 6

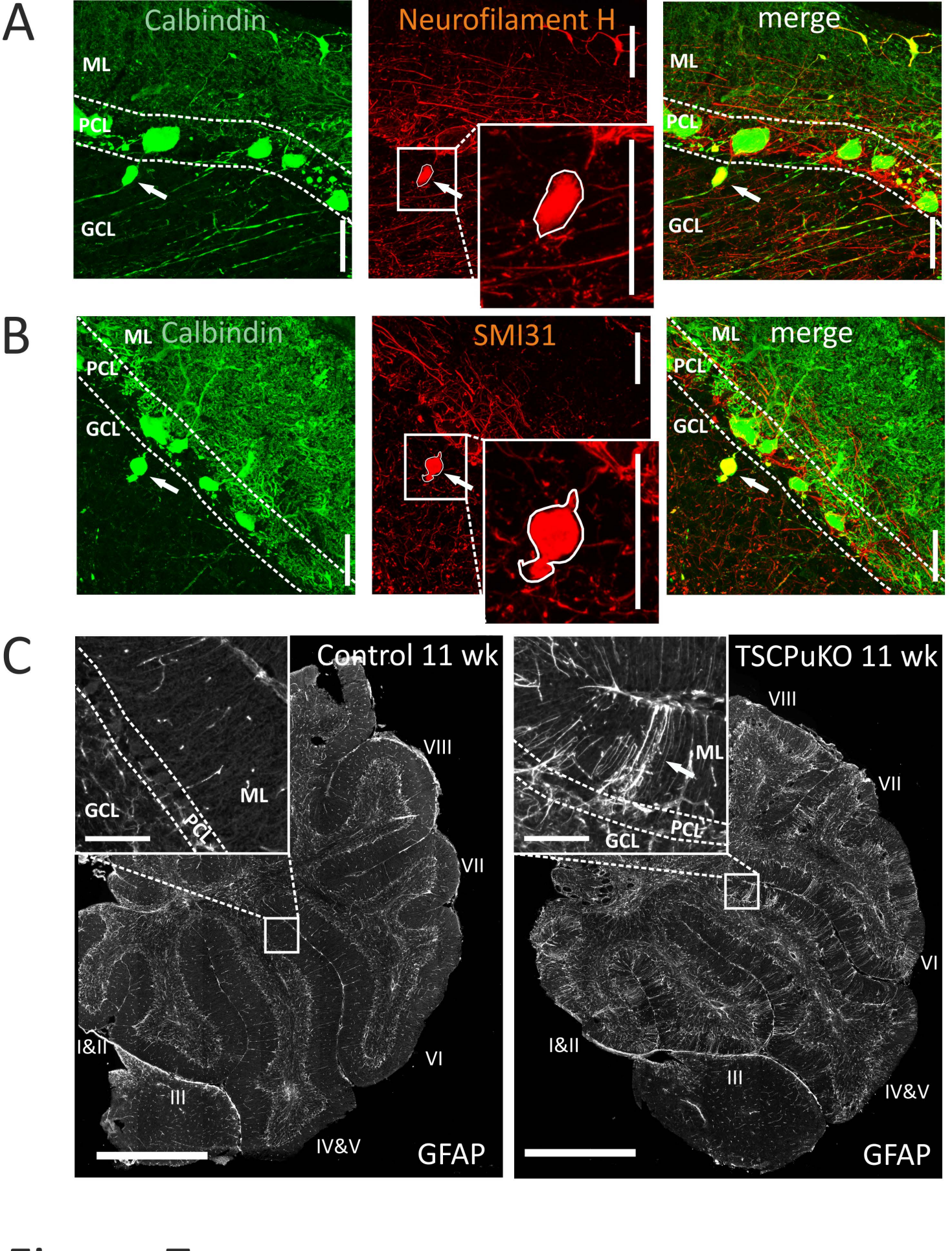
A
Calbindin
ML
PCL
GCL
Neurofilament H
merge
B
Calbindin
SMI31
C
Control 11 wk
TSCPuKO 11 wk
VIII
VII
VI
IV&V
III
I&II
GFAP

Figure 7

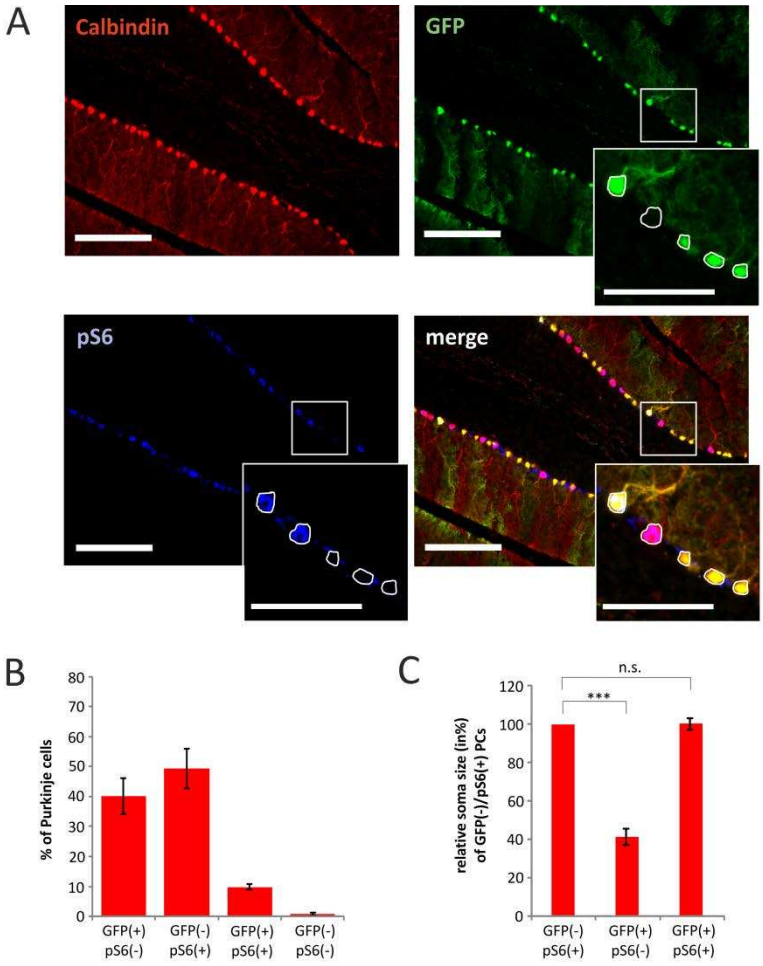

Supporting figure 1. Validation of pS6 as marker for raptor depletion in Purkinje cells. ***A***, Sagittal cerebellar slices of 11-week-old RAPuKO GFP mice were co-stained for the Purkinje cell marker calbindin (red), the GFP reporter (green) and pS6 (blue). The insert shows a representative sample of the different populations of Purkinje cells; somata are encircled in white. ***B***, Percentage of Purkinje cells expressing the different markers. Cells that underwent Cre-mediated recombination are GFP-positive and negative for pS6 [GFP(+)/pS6(-)]. Cells that never expressed Cre are GFP-negative and pS6-positive [GFP(-)/pS6(+)]. Less than 11% of the cells express GFP and are pS6-positive [GFP(+)/pS6(+)] or are double negative [GFP(-)/pS6(-)]. Purkinje cells of cerebellar lobes IV & V of 3 RAPuKO GFP mice were used for quantification. ***C***, Soma size of the Purkinje cells expressing the different markers relative to the soma size of GFP(-)/pS6(+) cells. Bars represent mean ± SEM for n =

3 mice. Statistical analysis used one-way ANOVA with Tukey's post hoc analysis. *P*-values: *** $P < 0.001$; ns $P \geq 0.05$. Scale bars: 200 μm (*A*), 100 μm (inset of *A*).

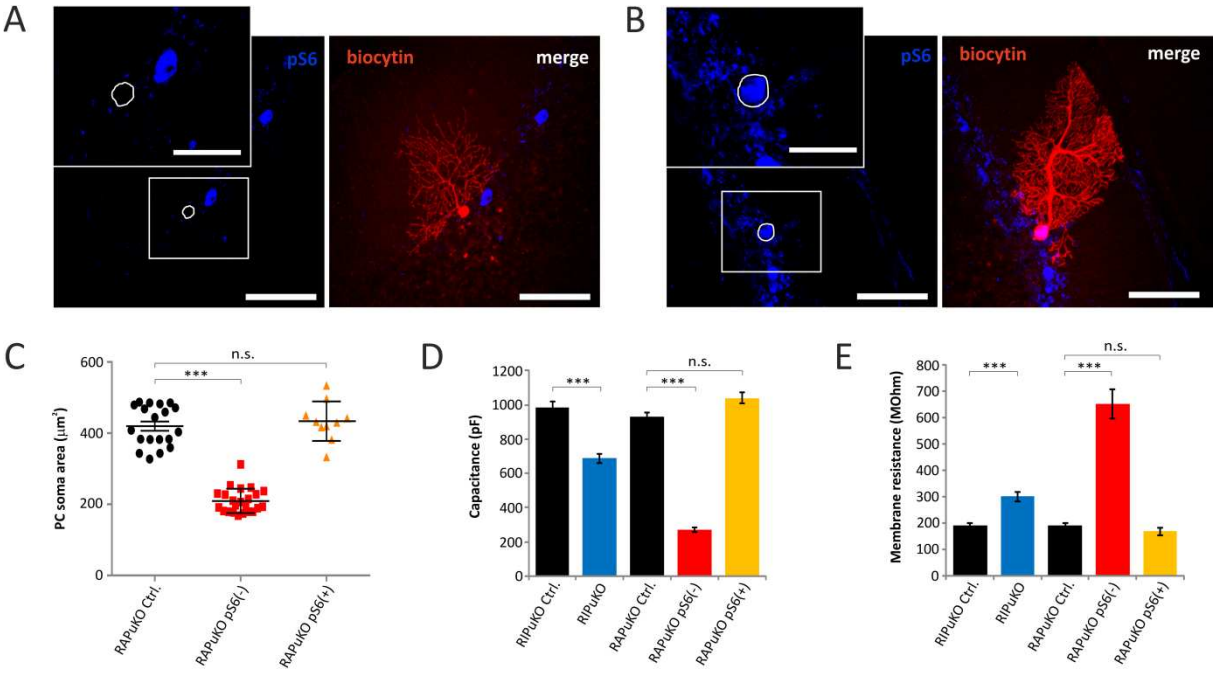

Supporting figure 2. Passive properties of rictor- and raptor-deficient Purkinje cells. ***A*** and ***B***, Fluorescence micrographs of biocytin-labelled Purkinje cells of 6-week-old RAPuKO mice that were detected by Cy3-streptavidin and co-stained for pS6. (*A*) pS6-negative and hence raptor-deficient Purkinje cell. (*B*) pS6-positive Purkinje cell. Note that this cell is bigger than that shown in (*A*). Pictures of (*A*) and (*B*) represent the projection of 122 or 86 confocal optical sections (voxel size: 0.38 x 0.38 x 0.5 µm), respectively. ***C***, Soma size of recorded Purkinje cells of control and RAPuKO mice. Projections of confocal sections of biocytin-labelled Purkinje cells as shown in (*A* and *B*) were used for quantification. ***D*** and ***E***, Capacitance (*D*) and membrane resistance (*E*) of Purkinje cells of 6-week-old RIPuKO, RAPuKO or corresponding control mice. n ≥ 9 Purkinje cells of n ≥ 3 mice were analysed for each genotype. Bars represent mean ± SEM. A two-tailed Student's *t*-test or a one-way ANOVA with Tukey's post hoc analysis was used for statistical analysis of RIPuKO or RAPuKO mice, respectively, in (*C* - *E*). *P*-values: *** $P < 0.001$; ns $P \geq 0.05$. Scale bars: 100 µm (*A* and *B*), 50 µm (insets of *A* and *B*).